Anti-phase clustering of regulatory factors shapes gene transcription burst

Bitong Li[1,2], Yew Yan Wong[1,3], Neftali Flores-Rodriguez[4], Tara Davidson[1], Matthew S Graus[1,3], Valeriia Smialkovska[5], Hiroaki Ohishi[6], Angelika Feldmann[5], Hiroshi Ochiai [6]† and Mathias Francois[1,2,7]†

[1] Centenary Institute, The University of Sydney, Royal Prince Alfred Hospital, Missenden Rd, Sydney, New South Wales, 2006, Australia.

[2] Department of Molecular Medicine, School of Biomedical Sciences, The University of New South Wales, Sydney, New South Wales, Kensington, 2052, Australia.

[3] The Genome Imaging Centre, Centenary Institute, The University of Sydney, Royal Prince Alfred Hospital, Missenden Rd, Sydney, New South Wales, 2006, Australia.

[4] Sydney Microscopy and Microanalysis, The University of Sydney, Sydney, New South Wales, 2006, Australia.

[5] German Cancer Research Center (DKFZ), Im Neuenheimer Feld 581, 69120 Heidelberg, Germany.

[6] Division of Gene Expression Dynamics, Medical Institute of Bioregulation, Kyushu University, Fukuoka, Japan.

[7] School of Medical Sciences, Faculty of Medicine and Health, The University of Sydney, Sydney, New South Wales, 2006, Australia.

†Correspondence should be address to

Hiroshi Ochiai (Tel: +81-92-642-6882)
ochiai.hiroshi.403@m.kyushu-u.ac.jp

Mathias Francois (Tel: +61 28627 9497)
m.francois@centenary.org.au

One-sentence summary: Temporal clustering of SOX2 at the *Nanog* gene locus reveals a regulatory layer in transcription

Keywords: transcription burst, SOX2 transcription factor, clustering dynamics, gene locus, RNA elongation, real-time imaging, single molecule, stem cell, enhancer

Abstract

The ability of stem cells to divide and self-renew depends on a complex choreography of molecular events that maintain the transcriptional oscillation of pluripotency genes. Only a handful of transcription factors (TFs) are necessary to preserve pluripotency and reprogram differentiated cells into stem cells. Paradoxically, while the protein players are known, the challenge remains to decipher the series of steps that TFs undertake to modulate "on" and "off" fluctuations of gene transcription. In this study, we employ a trimodal imaging approach that integrates single-molecule tracking of SOX2 mobility, *Nanog* locus diffusion, and real-time *Nanog* mRNA synthesis (STEAMING-tag reporter) to observe the coordinated activity of this molecular machinery. This combined system uncovered the temporal clustering dynamics of endogenous SOX2 occupancy at the *Nanog* locus and reveal how these dynamics relate to both transcriptional activity and the underlying chromatin behaviour in live embryonic stem cells. We link different types of SOX2 binding modes to roles in both transcriptional activation and termination or nucleosome repackaging. This redefines a dual function for SOX2 at the same gene locus during both gene expression and silencing processes. This work exposes a new layer of TF regulation, indicating a priming role rather than direct transcription initiation directly relevant to mammalian stem cell biology.

Main text

The exquisite regulation of gene expression in space and time dictates cell fate decisions and lineage specification at the molecular level. Two components are essential to this process: 1) the communication between genome regulatory regions, including promoters and enhancers; 2) a molecular machinery able to coordinate the activity of the genome control panel. The latter include transcription factors (TFs) that regulate messenger RNA (mRNA) synthesis in *trans* via binding to DNA *cis*-regulatory elements.

Recent progress in imaging and single-cell analysis technologies has revealed that transcription, production of RNA molecules from a corresponding gene, occurs in a discontinuous and dynamic manner. Nascent mRNA synthesis oscillates between sustained production in an "on" state and minimal synthesis in an "off" state [1]. The timescale of this on-and-off cycle varies between genes but typically ranges from several minutes to hours [2]. While transcriptional activity dictates the levels of gene mRNA synthesis, the relationship between TFs dynamics and transcription burst kinetics is not yet fully understood.

TFs activity is highly dependent on chromatin region accessibility, DNA affinity and the recruitment of cell-type specific co-factors [3–5]. In addition, multiple biophysical constraints shape TFs mobility and fine-tune their behaviour. TFs move through a complex chromatin landscape, which displays a sophisticated higher-order organisation. Importantly, TFs navigate a crowded environment while eliciting interactions with different classes of molecules, such as proteins, RNA, and DNA. Recent advances in high-resolution imaging, such as single-molecule tracking (SMT) [6–9], have revealed key biophysical features, such as a diffusion rate or confined mobility, that drive TF-specific activity. These quantifiable behaviours have determined TF search pattern mechanism, offering new insights into TF biology, on how a TF select its target gene. For instance, a landmark study has demonstrated, that SOX2, which is essential for stem cell pluripotency, searches for a specific target through the

combination of diffusion and sliding [10]. Different diffusion rates of SOX2 were shown to modulate asymmetric gene expression programs during early embryo formation, limiting stem cell fates to either extra-embryonic annexes or the embryo proper [11]. Despite a clear role for TF biophysical parameters in controlling cell fate decision, there is still a gap in our understanding of how these behavioural features directly contribute to the modulation of gene expression levels.

To unravel the mechanisms that underpin the dynamics of transcriptional activation, it is critical to be able to determine the TF/DNA binding kinetics requirement and establish a functional relationship of this characteristic with the nascent mRNA synthesis rate. Despite important findings brought with SMT-based methods, they have several limitations. Firstly, it is difficult to biologically interpret the activity kinetics of different TF molecule sub-populations (e.g. different types of confined mobility). Furthermore, the lack of sequence specificity of SMT-based techniques is not sufficient to determine the precise chromosomal coordinates of TF interaction.

To overcome these limitations, complementary methods that capture genome locations have been used to assess the activity of a protein of interest in a specific region. Some studies based on locus-centric approaches have taken advantage of anchor-based genetic reporter systems to label specific genome locations [12]. While this approach enables the visualisation of specific DNA regions and the analysis of protein behaviour through SMT, the information about these regions, such as whether gene transcription is on or off, remains obscure. As a result, it is difficult to discriminate between how a specific molecular behaviour is functionally related to a specific step in the transcription cycle.

Investigating the relationship between TF binding kinetics and the rate of transcriptional activity is complicated by significant differences in the timescales of these two biological processes. We addressed this challenge by using a multimodal imaging approach that enables us to explore the

coordinated activity of regulatory factors and nascent mRNA synthesis at a specific gene locus in live cells, or by measuring them correlatively in fixed cells.

In this study, we use the *Nanog* gene locus, well known to exhibit robust transcriptional bursts [13], as a proof-of-principle that it is possible to quantify its coordinated transcriptional activity along with its direct regulator, the SOX2 TF, in real-time in pluripotent stem cells. Importantly, SOX2 has been shown to directly regulate *Nanog* transcription to maintain pluripotency with both its loss- and gain-of-function leading to impaired *Nanog* expression [14–18].

We have achieved this by combining STREAMING-tag and SMT-based imaging techniques. While STREAMING-tag reporter system allows for profiling of locus mobility and transcription bursts at allelic resolution via labelling with different fluorescence markers [19], SMT provides a readout of TF behaviour at the locus of interest. This work provides a time-based picture of multifaceted SOX2 behaviours linked to distinct phases of the *Nanog* gene locus transcription cycle.

Multi-modal microscopy to quantify SOX2 occupancy at the *Nanog* gene locus relative to its transcriptional on-state

To address the main limitation of converting biophysical observations into a relevant biological interpretation in the context of TF mobility and gene transcription, we opted for a paired measurement that combines two live imaging methods: SMT and the STREAMING-tag reporter system. To measure TF long dwell times on the chromatin (e.g. over 4 sec or more) also known as confined mobility in parallel with processive transcriptional stages, we used a multimodal imaging platform. The assessment of STREAMING-tag reporter activity via Spinning Disk Confocal (SDC) module allows us to measure nascent mRNA synthesis and locus mobility, while the slow tracking SMT using the HILO module displays TF chromatin occupancy dynamics at a single locus resolution (see Methods). This readout gives access to TF behaviours at a gene-specific locus relative to mRNA nascent transcription and allows quantifying TF binding dynamics and dwell time relative to the "on" and "off" states. This approach was established in mouse embryonic stem cells (mESCs) by introduction of the STREAMING-tag reporter cassette (MS2 and TetO repeats) at the *Nanog* locus with expression of reporter proteins (MCP-RFP and mTetR-GFP), and the SNAP-tag knocked-in into either the *Sox2* or *Brd4* locus [19] (fig. 1a).

Previous studies on fixed cells using super resolution-based approaches have shown that around 10 to 20 molecules of regulatory factors cluster on enhancers scaffolds that come into proximity of their target gene locus [20,21]. In this study, we also opted for the term "clustering" to acknowledge the potential influence of protein oligomerisation and/or protein/RNA aggregates on the observed dynamics of TF occupancy, in addition to binding at specific sites.

To further validate the dynamics for this type of SOX2 behaviour in our reporter system, we performed a simultaneous two-colour SMT experiment with sparse labelling (JF549) in one channel and saturated labelling (JF646) in another channel in the same cells (supp fig. 1a-c). Fluctuations in

fluorescent signal intensity under saturated labelling conditions were used to construct masks to define regions of different SOX2 concentration, with high as the top 8%, following 30% as medium and the remaining signal as low (see Methods). The sparse SOX2 labelling signal was overlaid onto the mask to assess the dark fraction contribution to individual SMT-detected molecules (supp fig. 1b and c). This approach further confirm work on fixed cells and suggests that on average over 50% of the SMT-detected SOX2 molecules may accumulate in clusters of high or medium intensity. This indicates that most imaged single SOX2 molecules are involved with foci made of at least two or more SOX2 molecules (supp fig. 1c and video supp 1).

Because TF chromatin occupancy dynamics occur on a shorter time scale (seconds) compared to transcription bursts (minutes), we chose a two-step measurement method that continuously monitors SMT interspersed with a regular assessment of transcriptional activity at the *Nanog* locus. To accomplish this, we utilised a dual image acquisition technique that discriminates between SOX2 chromatin binding dynamics and *Nanog* mRNA elongation kinetics (3 minutes) (fig. 1b, image acquisition mode 1). This imaging approach relies on continuously measuring by SMT for 30 frames (exposure time 500 ms, no interval time), alternating with 1 frame that records both GFP and RFP signals over a 3-minute period. Fluorescent beads were used to evaluate the changes in light path occurring between shifts from SDC to HILO modalities. Post-image acquisition, we applied a custom script to correct for image misalignment (see Methods) (supp fig. 2a-f). The STREAMING-tag system has been designed to denote transcription at a gene locus. This is done through tagging a specific gene locus with a GFP signal and actively transcribed mRNA with RFP. With this reporter system, the presence of a GFP-only signal denotes that the transcription of the *Nanog* locus is "off". Co-localisation of the GFP and RFP spots within a 440 nm region of interest (ROI, 4-pixel radius) determines that nascent *Nanog* transcription is occurring, defining an “on” state. Of importance, the STREAMING-tag cassette is knocked at around 300 bp downstream from the transcription start site

(TSS), while transcriptional pausing has been shown to occur about 50-60 bp downstream of the TSS [22–24]. Therefore, with the STREAMING-tag reporter system, only the productive transcription after pause-release is observed (supp fig. 2g). This means that the "off" state, as we define it in this study, also includes the early steps of transcriptional initiation up to the release stage. The "on" state enables the detection of nascent mRNA produced during transcriptional elongation. When the RFP signal is lost, this means that splicing has occurred, or termination has been completed.

To measure the SOX2 occupancy dynamics in a locus-specific manner while *Nanog* is in an "on" state (fig. 1c), we used an ROI of 4-pixel radius, (440 nm) that centres on the GFP spot when both GFP and RFP signals are detected (fig. 1d and e). Such a distance was defined based on the previous observation that elevated concentration of regulatory factors around the *Nanog* locus ranges between 200 and 400 nm [19,21]. Unsurprisingly, we find multiple locations with SOX2 enrichments all throughout the nucleus (fig. 1d). Interestingly, within 440 nm of the GFP detection, we systematically observe an enrichment of SOX2 events (fig. 1e), suggesting that clustering activity is temporally correlated with the *Nanog* locus activity.

Distinct types of SOX2 occupancy dynamics at the *Nanog* gene locus during on and off-state

Here, we measured the SOX2 visiting frequency at the *Nanog* locus to determine its clustering dynamics profile while the transcription is "on". It revealed distinct modes of occupancy that occur at different rates throughout transcription elongation (fig. 2a and b and video supp 2). The first mode indicates no to low clustering (fig. 2a), while the second shows persistent locus occupancy of moderate intensity (fig. 2b).

It is known that the SOX2 protein binds to enhancers at the *Nanog* locus to induce transcriptional transactivation [25,26]; however, the timing of this event in relation to transcription cycle remains elusive. Hence, to understand how SOX2 clustering dynamics correlates with the timing of

transcription burst, we next set out to evaluate the occupancy rate of this TF during the "off" state period.

The assessment of SOX2 visiting frequency while the locus is not actively transcribing RNA uncovers a third type of occupancy behaviour characterised by a high rate of visiting events over a short number of frames (fig. 2c-e and video supp 3, video supp 4 and video supp 5). Quantitation of the different types of temporal clustering kinetics (fig. 2f) revealed that low to medium visiting frequency are the most prevalent at both on and off state, and that a discrete population of SOX2 molecules display high clustering activity only at off state. These different clustering activities indirectly reflect possible varying oligomeric status and recruitment of specific protein partners as well as random interaction with RNA products, all likely to influence this TF high-frequency clustering activity [20,27–30].

To show that the different SOX2 clustering activities are not restricted to the *Nanog* locus only, we took advantage of the dual SMT dataset described above to analyse the presence of different types of visiting frequency relative to the fluctuation of SOX2 local concentration across the nucleus. This analysis has shown that all three types of clustering activity (low, medium and high) are broadly detected across the nucleus in regions that show elevated SOX2 concentrations (supp fig. 3a). Quantitation of these three types of visiting frequency revealed that, the occurrence of high SOX2 clustering is a broad mechanism used on a genome-wide scale most likely across many gene loci (supp fig. 3b).

As we have shown above, SOX2 occupies the *Nanog* gene locus more frequently when transcription is in "off" state. To further explore the relationship between SOX2 and RNA Polymerase II, we quantified the rate of co-localisation between the transcriptionally active form of RNA Pol II (phospho-Ser5 RNA Pol II) and SOX2 clusters using dSTORM super-resolution microscopy. This approach indicated that on average SOX2 cluster population co-localises (cluster centre mass to centre mass, d < 50 nm) with active RNA Pol II foci at a low rate (5%, supp fig. 4a-c). Additional analysis determined that active RNA Pol II is mostly in presence of a vast majority of SOX2 clusters

that are the smallest one detected (< 1 μm) (supp fig. 4d). The findings from both types of imaging approaches revealed the spatiotemporal activity of SOX2 during transcription elongation. Mainly, SOX2 visiting frequency increases while elongation is off, which results in small SOX2 cluster sizes when active RNA Pol II is near.

Chromatin organisation and epigenetic modifications both play important roles in the activation of transcriptional initiation and are modulated in a cyclical, stepwise fashion. These periodic series of ordered and coordinated molecular events have been included in the theoretical modelling of transcription [31–34]. Further, a mathematical model proposed a molecular framework for the transition between "off" and "on" states that considers transcriptional activator residence time relative to the burst frequency [34]. Such a conceptual framework prompted us to assess SOX2 chromatin occupancy dynamics in relation to the progression through a full cycle of transcription.

High SOX2 clustering frequency is anti-phased with *Nanog* mRNA elongation

Based on the population average of SOX2 long dwell time in mESC (4-5 sec, supp fig. 5) [11,35], and the average time of transcription burst at the *Nanog* locus (3 min) [13], we designed a second mode of acquisition to image continuously through a full transcription cycle (fig. 3a, image acquisition mode 2). Briefly, this approach alternates confocal imaging of the *Nanog* locus for 3 seconds and SMT measurement for 500 ms with a repeat of this cycle over 9 minutes (150 cycles total, see Methods, video supp 6). Such a design allowed us to infer that a detected SOX2 molecule (long-dwell time ≥ 4 sec) prior to and after the *Nanog* locus imaging is the same molecule. To be conservative, in addition to the detection of long-lived fraction (2-frame detection, supp fig. 6a, schematic), we classified SOX2 short dwell time events that corresponded to the capture solely over one frame period (supp fig. 6b, schematic). This approach enables us to measure the presence of SOX2 clusters that persist near the *Nanog* locus over time.

To fully cover a complete event of transcription burst, we analysed SOX2 survival rates during a period that encompasses a step of transcriptional elongation and its transition to a refractory period, until the nascent RNA signal disappeared (fig. 3a). Analysis of SOX2 visiting frequencies with acquisition mode 2 over a 9-minute period while the *Nanog* locus is in off-state further confirmed the presence of the three types of occupancy rates (low, medium and high) reported above. The analysis of the number of SOX2 detected molecules and their relative survival rates at the *Nanog* locus revealed that, in addition to different types of visiting frequencies, SOX2 clusters display both short-lived and long-lived fractions (fig. 3b). From there it is possible to classify SOX2 clustering activity into three distinct types: type I - low to no clustering and short lived; type II - medium to high clustering and short lived; and type III - high clustering and long lived (fig. 3b and supp fig. 7).

To further understand the relationship between the temporality of SOX2 occupancy and mRNA synthesis, we next imaged the activity of a well-known elongation factor, the BRD4 protein. Here, we used a reporter cell line that harbours the STREAMING-tag reporter system combined with a SNAP-tag that has been knocked into the *Brd4* locus [19] and employed the imaging acquisition mode 2 described for SOX2. This approach revealed that BRD4 occupancy is mostly concurrent with nascent mRNA production (fig. 3c and supp fig. 8) [19]. Importantly, this approach further confirmed that the long-lived and highly active SOX2 clustering dynamics (type III) is out-of-phase with the elongation step that involves BRD4 and RNA polymerase II activity (fig. 3d and supp fig. 9).

Since earlier studies showed that open chromatin regions drift relatively slowly compared to closed ones that diffuse faster [19,36], this prompted us to investigate further how SOX2 occupancy behaviours affect the *Nanog* locus mobility.

To refine the temporal hierarchy between the distinct types of SOX2 behaviours and transcriptional elongation, we measured changes in *Nanog* locus mobility in relation to the presence or absence of SOX2 occupancy. This quantitative approach revealed that the *Nanog* locus displays opposite diffusion kinetics that are correlated to different types of SOX2 residency profiles. During SOX2

occupancy type II, the *Nanog* locus harbours a slower diffusion rate while SOX2 is present compared to when there is no SOX2 detected (fig. 3e). Conversely, the locus diffusion kinetics increases in the presence of high SOX2 occupancy (type III) compared to when there is no SOX2 detected (fig. 3f). Recent, work from Platania and colleagues has shown that locus diffusion is a reliable predictor of enhancer to promoter contact [37], therefore, by combining information gained on change in locus mobility with occupancy rate measurement, we posit that SOX2 type II behaviour is associated with open chromatin state and occurs prior to active nascent mRNA synthesis. This is opposed to type III that is associated to a more compact chromatin state likely to follow the elongation step and related to nucleosome repackaging.

In addition to interacting with DNA, SOX2 has been shown to recruit RNA [28] and more broadly, TFs have been suggested to harbour an RNA-binding arm, which also influences their mobility [38]. Since this study shows that high SOX2 occupancy activity with longer dwell time at the *Nanog* locus occurs in the absence of *Nanog* nascent transcripts, this prompted us to investigate further the potential role of alternative RNA species such as enhancer RNAs (eRNAs) from well-characterised SOX2-dependent regulatory elements [26,28].

Nanog eRNAs are mostly transcribed at "off" state

eRNAs function involves stabilising chromatin loops and recruiting co-factor such as p300 and acting as a sponge for the negative elongation factor (NELF) [39]. Since their role in modulating transcription is a possible mechanism, this prompted us to specifically investigate the role of *Nanog* eRNAs involvement in the transcription cycle. The *Nanog* locus is one of the most well-characterised genomic regions in the context of embryonic stem cell pluripotency, with the presence of three super-enhancers that frame the gene body within a 100 kb region [40,41]. These regulatory regions are located at -5 kb, -45 kb, and +60 kb from the transcription start site (TSS), respectively [40] and are actively transcribed [42]. The functional hierarchy of these three enhancer regions in mESCs has been validated

using genome editing with -5 kb being the most critical one, -45 kb of modest influence and +60 kb with no impact on the expression [41]. Using enhancer transcription as a proxy for TF activity at these regulatory regions, we interrogated the presence of eRNAs molecules in relation to *Nanog* nascent transcripts. For this, we employed an RNA-FISH method to map eRNAs and transcribed *Nanog* introns in parallel with the STREAMING-tag reporter as a readout of elongated *Nanog* expression. We devised an approach for quantifying eRNA/nascent mRNA expression in a high-throughput manner over thousands of cells (supp fig. 10).

Taking advantage of GRO-seq datasets [40], we designed probe sets that detect both sense and/or anti-sense eRNA strands for each of the three *Nanog* enhancers (fig. 4a). This analysis revealed that the expression of at least one or more sense or anti-sense eRNAs occurs in more than 80% of the stem cell population (fig. 4b). Co-expression of all three eRNAs was observed in approximately 15-20% of the cells (fig. 4b), with the +60 kb region being by far the most highly transcribed enhancer on the anti-sense strand (70%) as opposed to 30-35% for the -45 kb and -5 kb (fig. 4b). Pairwise analysis of each combination of eRNAs (sense and anti-sense) revealed that at least 30% of the stem cell population co-express an eRNA pair, with a set of sense eRNAs (+60 kb/-5 kb or +60 kb/-45 kb) being co-expressed in around 15% of the cells. Due to eRNAs rapid degradation rate, these co-expression events suggest that enhancers were probably transcribed almost simultaneously.

The analysis of chromatin conformation by Capture-C has demonstrated the contacts between *Nanog* promoter and all three enhancers (supp fig. 11), allowing us to posit that eRNA co-localisation may be correlated with a co-activation of their transcription in the proximity of the *Nanog* gene locus. To further assess whether transcription at these enhancers occurs synergistically, we quantified the co-localisation of these eRNAs either by pair or for all three transcripts (fig. 4c). This analysis reveals that all pairs tested display (5-15%) of sub-nuclear co-localisation. In some instances, co-localisation was also found for all three eRNAs for both the sense and anti-sense strands (fig. 4c-d). Altogether,

these data suggest that transcriptional activity of *Nanog* enhancers is synchronised within a scaffold region for at least 30-45% of the mESCs population.

To explore the temporal coordination between *Nanog* eRNA transcription and nascent mRNA production, we next investigated the expression of eRNAs relative to the *Nanog* active transcription. All three eRNA transcripts exhibit a positive correlation between their expression and the accumulation of endogenous *Nanog* introns products (fig. 4e). By contrast, regardless of the transcriptional direction of eRNAs, the quantitation of eRNAs' co-localisation with *Nanog* mRNA showed that only a small number of enhancer transcripts are present during the synthesis of *Nanog* nascent RNA (fig. 4f and supp fig. 12, - 45kb eRNA), suggesting that transcription of enhancer and gene body does not occur at the same time. Because the co-labelling of *Nanog* eRNAs and *Nanog* mRNA introns has limitations in defining the order of steps between these two transcriptional events, due to a possible intron retention mechanism [43], we further refine the temporal relationship of their synthesis using eRNA RNA-FISH combined with RFP detection from the STREAMING tag cassette. This enables us to quantify more accurately the abundance of *Nanog* enhancer transcripts in relation to the progression of *Nanog* elongation (fig. 4g and h). This approach shows that in the “on” state, while nascent *Nanog* mRNA is actively produced, eRNA presence is rarely co-detected for any of these enhancers. By contrast, in the “off” states, there is a wide range of eRNA molecules found in the nucleus (fig. 4g and h), suggesting that the timing of enhancer transcription is not concurrent to the one of *Nanog* mRNA elongation. This finding on the asynchronous activity of between enhancer and gene body RNA synthesis is consistent with a previous report suggesting that proximal enhancer transcription is mutually exclusive with gene body transcription [44].

SOX2 has been shown to directly recruit *Nanog* enhancers [25,41,45], however, the timing of this recruitment relative to transcriptional activation was unclear. Therefore, combining live observations of its clustering dynamics with eRNA quantitation relative to *Nanog* mRNA elongation, we propose

that the enhancer transcription surge coincides with SOX2's densest clustering activity while the gene locus is in a "off" mode.

In conclusion, our findings strengthen the link between the *Nanog* gene transcription cycle and the activity of its regulatory factors by integrating spatial and temporal SOX2 and BRD4 clustering dynamics, locus mobility, and enhancer transcription. This study establishes that SOX2 temporal clustering is out-of-phase with the active basal-transcriptional machinery to determine either the basis of permissive transcriptional "off" state that precedes transcription burst or a step that contributes to elongation termination (supp fig. 13, model).

Discussion

Previous studies have provided insights into transcription factor (TF) binding dynamics during active transcription, primarily focusing on yeast (e.g., Gal4/Gal10 system) [46] and mammalian cells with nuclear receptors like the glucocorticoid receptor (GR) on an exogenous MMTV promoter [47]. The Gal4-Gal10 system is a valuable model for understanding basic principles of transcriptional regulation, but transcription in yeast is often more straightforward due to fewer regulatory layers since the enhancer network is far less complex. By contrast, here we shed light on how the complex architecture of the endogenous *Nanog* locus shapes TF occupancy throughout the transcription cycle.

Platania et al., [37] have recently reported that gene locus diffusion is a better indicator than Hi-C genomics to predict enhancer to promoter distance. Our approach using the STREAMING-tag reporter system enables a unique integration of locus diffusion data alongside transcriptional activity, enhancing the discovery of SOX2 clustering roles when chromatin is in different states. Findings from this study reveal that SOX2 clustering behaviour is temporally distinct across different transcription cycle stages a temporal resolution which could not be achieved in previous work [46–49].

The TF occupancy pattern in yeast model system is typically synchronous with transcription bursts. Here, we observed an anti-phased relationship between SOX2 occupancy and the elongation phase, supporting emerging evidence of an inverse relationship between enhancer-bound condensates and active transcription [50]. Unlike Du et al., who focused on basal transcriptional machinery condensate dynamics (e.g., RNA Pol II, Mediator) at the *Sox2* locus, our work directly investigates the pioneer TF SOX2. This distinction is critical, as SOX2's regulatory function and influence on chromatin accessibility represent a more specialised aspect of gene regulation, distinct from the broader transcriptional machinery dynamics. Thus, our study offers a novel perspective on SOX2's specific contributions to transcriptional regulation and chromatin dynamics.

Our study demonstrates that SOX2 medium and high intensity-clustering activities at the *Nanog* gene locus frame transcription burst events and do not appear to directly cooperate with the BRD4-associated elongation step. This finding fits with the observation that, in stem cells, SOX2 gain-of-function leads to a reduction in *Nanog* mRNA levels and a loss of pluripotency [14,17]. In that instance, overcrowding of the *Nanog* locus may interfere with the elongation kinetics that does not require frequent SOX2 occupancy, disturb the pre-mRNA splicing [51] and derail the cycling pace of *Nanog* transcription required to drive pluripotency. Intriguingly, we observed a SOX2 oscillatory behaviours akin to the GR molecular behaviour previously reported [47], however, for SOX2 this occurs independently of ligand activation or hormonal cues. This is an unexpected finding, as neither an endogenous ligand nor any pulsatile regulation has been identified to control SOX2 activity. Our finding suggests the existence of a ligand-independent mechanism governing the clustering and oscillatory dynamics of developmental TFs like SOX2.

The observation of different locus mobility responses observed during the "off" state in the absence or presence of SOX2 clusters, is consistent with the observation that binding of the NuRD repressor complex increases *Nanog* locus mobility through nucleosome repackaging [52]. Since it has been shown that SOX2 and NuRD interact [53,54], it is tempting to speculate that SOX2 type III clustering behaviour that occurs post-elongation might be associated with NuRD and might contribute to chromatin compaction of that region. More broadly, these distinct SOX2 clustering activities are likely to indirectly represent changes in protein partners, variations in RNA concentration and chromatin epigenetic state at the locus that modulate SOX2 occupancy behaviour [10,28,55–57].

This study further informs earlier work that found a role for the interaction between SOX2 and RNA [28] and the finding that most TFs have an RNA-binding arm that helps generate an RNA-containing condensate that affects the diffusion and dwell time of genome effectors [38]. Interestingly, the transcription of *Nanog* enhancer RNA adopts a temporal pattern akin to SOX2 high-clustering

activities, with low to no expression during the elongation stage but higher concentration while the locus is in an "off" state. This observation suggests that SOX2 TF has to keep operating at the *Nanog* locus in an environment continuously crowded with RNA, either in the presence of eRNA or mRNA. Yet, SOX2 occupancy dynamics at the *Nanog* locus display multiple behaviours (type I-III), depending on whether elongation is "on" or "off" and whether it is preceding or occurring after the elongation step. This means that different types of RNA at the gene site, which change in concentration over time, are critical in determining how SOX2 behaves [28,38]. Here, we provide multiple lines of evidence that different SOX2-dependent molecular reactions represent varying "off" states at the *Nanog* locus region. These molecular reactions involve eRNAs, which have been shown to shape chromatin loops and recruit co-activators [39,58,59], likely influencing transcriptional output *Nanog* in a cooperative manner with SOX2 clustering dynamics.

In conclusion, we posit that cell-to-cell *Nanog* transcriptional fluctuation may be driven by asynchronous variations of SOX2 occupancy dynamics, eRNA levels, and mRNA bursts frequencies, producing a continuum of *Nanog* expression levels across the stem cell population. These varying synchronicities between genome effectors may give rise to a range of transcription rates, leading either towards self-renewal or differentiation.

Method

Cell lines

5 Genetically modified (STREAMING-tag knocked-in) mESCs were cultured as described [19]. In brief, all mESC lines were cultured in 2i medium (Knockout Dulbecco's modified Eagle's medium [DMEM, Thermo Fisher Scientific Australia Pty Ltd, AU, 10829018]; 15% fetal bovine serum [FBS, Thermo Fisher Scientific, USA, 16141079]; 0.1 mM 2-Mercaptoethanol [Sigma-Aldrich, USA, M3148-25ML]; 1×MEM nonessential amino acids [Thermo Fisher Scientific Australia Pty Ltd,
10 11140050]; 2 mM L-glutamine solution [Thermo Fisher Scientific Australia Pty Ltd, 25030081]; 1,000 U/mL leukemia inhibitory factor [Sigma-Aldrich, ESG1107]; 20 μg/ml Penicillin-Streptomycin [Thermo Fisher Scientific Australia Pty Ltd, 15140122]; 3 μM CHIR99021 [Sigma-Aldrich, SML1046-5MG]; and 1 μM PD0325901 [Sigma-Aldrich, PZ0162-5MG]) on 0.1% gelatin (Sigma-Aldrich, G1890-100G)-coated T25 flasks at 37°C and 5% CO_2.

15 HaloTag-Human SOX2 KI cell line (HaloTag-hSOX2 KI cell), in which the endogenous single exon *Sox2* is biallelically replaced with *hSOX2* cDNA, were established using CRISPR-Cas9 expression vectors (https://benchling.com/s/seq-5qSmelnJy4kN3pPttBor?m=slm-Mcd0jPctZwhu5s453hCC; https://benchling.com/s/seq-wGlQp3vgsvlH7GJPB4Hn?m=slm-xz8aFivYu18VyIbZ81co) and a targeting vector (https://benchling.com/s/seq-63w0RtPOOFpQKTe1Xb25?m=slm-
20 Bri31KJayf3dpQUFsIzX). C57BL/6NCr mESCs (derived from inbred mice, C57BL/6NCr, Japan SLC, Hamamatsu, Japan; 1.25×10^5) were conditioned in 2i medium and plated onto gelatin-coated 24-well plates. After 1 hour, the cells were transfected using Lipofectamine 3000 (Life Technologies, Gaithersburg, MD, L3000015) with 250 ng of the targeting vector, 400 ng of each CRISPR vector, and 75 ng of pKLV-PGKpuro2ABFP (puromycin resistant, Addgene, plasmid #122372), following
25 the manufacturer's instructions. Puromycin (1 μg/ml) was added to the 2i medium 24 hours post-transfection for selection. The medium was replaced every 2 days, with the first exchange occurring 24 hours after puromycin addition. Seven days post-transfection, cells were treated with 300 μM

JFX_{549}-Halo-Tag ligand for 30 minutes, followed by three washes and a 30-minute culture in 2i medium. Cells were then trypsinised, analysed via FACS, and Halo-Tag-positive cells were sorted and seeded onto a gelatin-coated 6-cm dish. The medium was changed every 2 days. One week after sorting, 16 colonies were picked for downstream analysis and gene targeting verification. Polymerase chain reaction (PCR) was conducted using primers outside the homology arms, and clones that appeared to have successful biallelic knock-in were selected. These candidate clones underwent further analysis by Southern blotting. This cell line was maintained in 2i medium on 0.1% gelatin.

HCR™ RNA-FISH

mESCs (1×10^5) were seeded onto a laminin 511 (BioLamina, Sweden, LN511-0502)-coated 8-well chambered dish (Ibidi, Germany, 80807-90) and cultured for 1.5 h at 37°C and 5% CO_2. Cells were washed with 1×Dulbecco's phosphate-buffered saline (DPBS, Thermo Fisher Scientific Australia Pty Ltd, 14190250) 3 times and fixed with 4% paraformaldehyde (Emgrid Australia, AU, 15710) for 10 min at room temperature (RT). Then, cells were washed twice with 1×DPBS and stored in 70% ethanol at - 30°C. After aspirating ethanol at RT, cells were washed with 2×SSC buffer (Molecular Instruments Inc., Los Angeles, CA, USA) and incubated with probe hybridisation buffer (Molecular Instruments Inc.) for 30 min at 37°C. Cells were then hybridised with 1.2 pmol of each probe set dissolved in probe hybridisation buffer at 37°C overnight. The excess probe was removed by washing the cells 5 times with probe wash buffer (Molecular Instruments Inc.) at 37°C. Then, cells were washed twice with 5×SSCT (Molecular Instruments Inc.) buffer at RT. After incubation in the amplification buffer (Molecular Instruments Inc.) for 30 min at RT, the cells were hybridised with 12 pmol of pre-heated and snap-cooled hairpin h1 and h2 probes for 3 h at RT in the dark. The excess hairpin probes were removed by washing the cells 5 times with 5×SSCT buffer at RT. The hybridised cells were incubated with Hoechst33342 (1:125, Thermo Fisher Scientific Australia Pty Ltd, R37605) for 3 min, washed 3 times with 1×DPBS and then stored in 1×DPBS for imaging. Imaging acquisition

was performed on a 3i Multimodal microscope (Intelligent Imaging Innovations, Inc., Denver, CO, USA) with a Spinning Disk Confocal (SDC) unit (CSU-W1, Yokogawa Electric Corporation, Tokyo, Japan), a 50 µm pinhole disk, a 100× 1.49 NA Oil Nikon HP TIRF objective (Nikon Instruments Inc., Melville, NY, USA) and a Prime 95B back illuminated sCMOS camera (Teledyne Photometrics, Tucson, AZ, USA), controlled by SlideBook software (Intelligent Imaging Innovations, Inc.). Far-red smFISH probes were imaged with a 640 nm excitation, a 630-644 nm dichroic and a 692/40 emission filter. Red smFISH probes were imaged with a 560 nm excitation, a 555-564 nm dichroic and a 617/73 emission filter. Green smFISH probes were imaged with a 488 nm excitation, a 485-493 nm dichroic and a 525/30 emission filter. Hoechst33342 was imaged with a 405 nm excitation, a 410-410 nm dichroic and a 445/45 emission filter. Images (512 by 512 pixels) were collected with a pixel size of 110 nm and with a Z-stack step size of 2.0 µm (typical range of 15 µm). Images were processed by Fiji software (NIH, Bethesda, MD, USA) [60] and analysed using the customised CellProfiler pipeline [61]. The smFISH spots of each illumination channel were quantified through the customised MATLAB pipeline [62]. smFISH probes were obtained from Molecular Instruments Inc.

mESCs (3×10^4) were seeded onto a 0.5% gelatin (Sigma-Aldrich, G1890-100G)-coated 30 mm round coverslip and cultured for 1.5 h at 37°C and 5% CO_2. smFISH staining was performed on cells as described above. Images were acquired using a laser scanning Nikon Eclipse C2 (Nikon Instruments Inc., Melville, NY, USA) confocal microscope, with a 100× 1.40 NA Oil Nikon objective, controlled by Nikon Imaging Software (NIS). A 640 nm laser was used to excite the Far-red smFISH probes (dichroic 405/488/564/640, emission filter 700/80), MCP-RFP was excited with a 560 nm laser line (dichroic 405/488/564/640, emission filter 595/40), a 488 nm laser was used to excite mTetR-GFP (dichroic 405/488/564/640, emission filter 525/50), and a 405 nm laser was used to excite the DAPI channel (dichroic 405/488/564/640, emission filter 447/60). A detector gains of 20 was used for the 640 nm channel; a gain value of 30 was used for the 560 nm labelled samples; the 488 nm channel was imaged using a gain of 25; a gain value of 23 was used for the DAPI channel. No frame

accumulation or frame integration was used. Offsets were kept at 0. A pinhole size of 60 µm was used. Pixel dwell time was 1.92 µs. Images (512 by 512 pixels) were collected with a pixel size of 90 nm. Images were processed by Fiji software data and then analysed through the customised CellProfiler pipeline. The GFP/RFP and smFISH spots of each illumination channel were quantified through the customised MATLAB pipeline. Of note, a large fraction of cells has a loss of mTetR-GFP spots after fixation, hence we strictly determined the on-state in presence of both RFP and GFP signal co-localisation.

Sequential smFISH and HCR™ RNA-FISH

Mouse ESCs derived from inbred mice (Bruce 4 C57BL/6 J, male, EMD Millipore, Billerica, MA, USA) (5×10^4) were seeded onto a laminin 511 (BioLamina, Sweden, LN511-0502)-coated 8-well chambered cover glass with #1.5 glass (Cellvis, Sunnyvale, CA, USA, C8-1.5HN) and cultured for 24 hours at 37°C and 5% CO_2. Cells were washed with 1× phosphate-buffered saline (PBS, Nacalai Tesque, 14249-24) three times and fixed with 4% paraformaldehyde (Wako Pure Chemical Industries, USA, 168-20955) for 10 minutes at RT. After fixation, cells were washed twice with 1×PBS and stored in 70% ethanol at - 20°C. Ethanol was aspirated at RT, and cells were incubated with 0.5% Triton-X in 1×PBS for 15 minutes at RT. Cells were then washed three times with 1×PBS. Blocking solution (1×PBS, 10 mg/ml UltraPure BSA [Thermo Fisher Scientific, AM2616], 0.3% Triton-X, 0.1% Dextran sulfate, 0.5 mg/ml UltraPure Salmon Sperm DNA Solution [Thermo Fisher Scientific, 15-632-011]) was added, and cells were incubated for 15 minutes at RT. After 1×PBS washing, cells were post-fixed with 4% formaldehyde in 1×PBS at RT for 5 minutes, followed by six washes with 1×PBS. Cells were incubated at RT for 15 minutes. Samples were then further post-fixed with 1.5 mM BS(PEG)5 (PEGylated bis(sulfosuccinimidyl)suberate) [Thermo Fisher Scientific, A35396] in 1×PBS at RT for 20 minutes, followed by quenching with 100 mM Tris-HCl pH 7.5 at RT for 5 minutes. Cells were washed with 1×PBS and 2×SSC buffer. Cells were then incubated with

probe hybridisation buffer (50% formamide, 10% dextran sulfate, 2×SSC, 10 nM each *Nanog* intron probes) for 24 hours at 37°C in a humidified chamber. Cells were washed with 55% wash buffer (55% formamide, 0.1% Triton-X, 2×SSC) for 30 minutes at RT and subsequently washed three times with 4×SSC buffer. Cells were incubated with 200 µL EC buffer (10% ethylene carbonate, 10% Dextran sulfate, 4×SSC, 100 nM readout probe, 150 nM secondary probe) for 20 minutes, followed by washing with 200 µL 4×SSCT buffer (4×SSC, 0.1% Triton-X). Cells were then washed with 200 µL 12.5% wash buffer (12.5% formamide, 0.1% Triton-X, 2×SSC) and 200 µL 4×SSC, followed by washing with 200 µL DAPI solution (4×SSC, 0.1% Triton-X, 5 µg/ml DAPI) for 30 seconds. Finally, cells were washed with 200 µL anti-bleaching buffer (50 mM Tris-HCl, 300 mM NaCl, 3 mM Trolox, 0.8% glucose, 10 µg/ml catalase [Sigma-Aldrich, C3155], pH 8.0) before imaging. Imaging acquisition was performed using a Nikon Ti-2 microscope with a CSU-W1 confocal unit (Yokogawa), a 100× 1.4 NA Nikon Plan Apo λ oil-immersion objective lens, and an iXon Ultra EMCCD camera (Andor Technology, Belfast, UK), with laser lines of 405 nm, 488 nm, 561 nm, and 637 nm. Z-stack images spanning 10 µm with 200 nm intervals (51 sections; 130 nm/pixel) were acquired.

Cells previously processed for smFISH were further subjected to HCR™ RNA-FISH staining, as described in the "HCR™ RNA-FISH" subsection. The hybridised cells were incubated with DAPI solution for 3 minutes, washed with anti-bleaching buffer. Imaging acquisition was performed using a Nikon Ti-2 microscope with a CSU-W1 confocal unit (Yokogawa), a 100× 1.4 NA Nikon Plan Apo λ oil-immersion objective lens, and an iXon Ultra EMCCD camera (Andor Technology, Oxford Instruments, Belfast, UK), with laser lines of 405 nm, 488 nm, 561 nm, and 637 nm. Z-stack images spanning 10 µm with 200 nm intervals (51 sections; 130 nm/pixel) were acquired.

Image processing was initiated using PyImageJ to perform several tasks [63]. First, smFISH images and HCR-FISH images of the same field of view were converted into a single hyperstack image to manage multi-dimensional image data efficiently. Subsequently, bleaching correction was applied to

minimise significant fluorescence intensity differences between the two experiments. Next, 3D drift correction was performed to compensate for any movement or displacement of the samples during image acquisition. The images were then subjected to maximum intensity projection. Following this, the "Extract SIFT Correspondences" and "bUnwarpJ" tools were used to correct for nuclear deformation between the two experiments. After these preprocessing steps, the nuclei were segmented using the Cellpose [64], which was specifically configured to identify nuclear regions. For spot detection, the Big-FISH [65] was employed. This involved several stages, including filtering the images to reduce noise using a Gaussian filter, detecting local maxima to identify potential spots, and applying adaptive thresholds to distinguish true signal spots from background noise. The detected spots were then masked using the nuclear segmentation results to ensure that only spots within the nuclear regions were considered.

dSTORM super-resolution imaging

HaloTag-hSOX2 KI mESCs (5×10^4) were transferred onto a laminin 511-coated 8-well chambered dish and cultured in 2i medium for 2 h. Cells were labelled with JF_{646}-Halo-Tag ligand (100 nM, LAVIS LAB, Ashburn, USA, NF-1-005) for 10 min at 37 °C, followed by washing with PBS three times. The samples were then fixed with 4% PFA at 37 °C for 10 minutes and then permeabilised with 0.03% Triton X-100 for 5 minutes followed by PBS wash. Samples were then blocked with 5% BSA/PBS for 30 minutes before staining with anti-human pSER5 (Merck Life Science, 04-1572), followed by secondary staining with anti-rat AF555 (Thermo Fisher Scientific, A78945). Finally, a post-fixation with 4% PFA was performed.

The fixed cells were imaged using the Everspark 1.0 imaging buffer (Idylle, Paris, France) with no gas exchange taking place. Cells were imaged on a Leica SR GSD 3D (Leica Microsystems, Wetzlar, Germany) with an iXon Ultra 897 EMCCD camera (Andor Technology, Oxford Instruments, Belfast, UK) and a 160× 1.43 NA Oil objective (Leica Microsystems, Wetzlar, Germany). The 642 channel

was imaged using a using a 642 nm excitation laser and a 642 HP-T filter (BP 642/10, 649, BP 710/100), the AF555 channel was imaged using a 532 nm excitation and a 532 HP-T filter (BP 532/10, 541, BP 600/100). Each channel was imaged sequentially starting with the far-red channel. Each channel was imaged for 25,000 frames at a 11.3 ms/frame rate. Localisation and clustering analysis were performed using Huygens Localiser (Scientific Volume Imaging B.V, Hilversum, Netherlands) [66]. The parameters used for particle identification: sigma = 1.25 and applied relative threshold > 2.1. The parameters used for particle localisation analysis: fit method = weighted least-squares and effective FWHM for fitting = 264 nm. Clustering analysis was performed using Huygens Localiser cluster analysis tool. Clustering was determined by DBScan with parameters of nearest neighbor = 10 and epsilon = 0.028 μm.

Live cell imaging

For live cell imaging, SNAP-tag SOX2 KI mESCs (5×10^4) were transferred onto a laminin 511-coated 8-well chambered dish and cultured in 2i medium for 2 h. Then, cells were incubated with JF_{646}-SNAP-tag ligand (5 nM, LAVIS LAB, Ashburn, USA, JBG-13-151) dissolved in imaging 2i medium (FluoroBrite DMEM [Thermo Fisher Scientific Australia Pty Ltd,. A1896701], 15% FBS [Thermo Fisher Scientific, USA, 16141079], 1× MEM nonessential amino acids [Thermo Fisher Scientific Australia Pty Ltd, 11140050], 2 mM L-glutamine solution [Thermo Fisher Scientific Australia Pty Ltd, 25030081], 1,000 U/mL LIF [Sigma-Aldrich, ESG1107], 3 μM CHIR99021 [Sigma-Aldrich, SML1046-5MG], 1 μM PD0325901 [Sigma-Aldrich, PZ0162-5MG]) for 30 min at 37°C and 5% CO_2 in the dark. The excess SNAP-tag ligand was removed by washing the cells 3 times with the imaging 2i medium. Cells were imaged in the 2i medium containing VectaCell Trolox Antifade Reagent (1:500, ABACUS DX, AU, CB-1000) and Hoechst33342 (1:125, Thermo Fisher Scientific Australia Pty Ltd, R37605). Time-lapses were acquired using a 3i Multimodal microscope (Intelligent Imaging Innovations, Inc., Denver, CO, USA) equipped with a CSU-W1 Spinning Disk

Confocal (SDC) unit (50 µm disk unit), a spinning TIRF (Vector2 TIRF, Intelligent Imaging Innovations, Inc.) unit, a high speed (3 ms) galvo port switcher (mSwitcher, Intelligent Imaging Innovations, Inc.) to select between SDC or HILO modalities, a 100× 1.49 NA Oil Nikon HP TIRF objective (Nikon Instruments Inc.) and Prime 95B back illuminated sCMOS cameras (Teledyne Photometrics). Microscope system was controlled by the SlideBook software (Intelligent Imaging Innovations). STREAMING-tagged reporters were imaged in SDC mode using the following filter settings: MCP-RFP was excited with a 560 nm laser line (dichroic ZT405/488/561/640tpc-uf1, emission filter FF02-617/73), a 488 nm laser was used to excite mTetR-GFP (ZT405/488/561/640tpc-uf1, emission filter FF01-525/30), and HILO SMT imaging was performed using a 640 nm laser, a Di03-R405/488/561/635 dichroic mirror and a FF01-692/40 for emission filter. For image acquisition method 1, the microscopy was set up first for SDC image acquisition (1 frame each, 300 ms camera exposure each channel, no delay time) and then shifted to the HILO-SMT module for slow tracking of fluorescent molecules (30 frames, 500 ms camera exposure, no delay time) to determine occupancy kinetics. The imaging cycle was repeated 10 times with a total duration of 3 min. For image acquisition method 2, one frame in HILO-SMT mode was acquired first using a camera exposure time of 500 ms, followed by the acquisition of 3 frames of the SDC channels (no interval time). The imaging cycle was repeated 150 times for 9 min.

TetraSpeck 0.5 µm fluorescent beads (Thermo Fisher Scientific Australia Pty Ltd, T7281) were used as fiducials to correct for camera misalignment between the SDC and HILO imaging modules. Beads were plated on a laminin 511-coated well with imaging 2i medium and imaged under the same conditions as described above (green and red beads were imaged using the SDC camera, dark-red beads were imaged using the HILO-SMT imaging settings). The shifted distance between the SDC channels (GFP and RFP) and the HILO-SMT channel was realigned based on the central position of the beads in each channel.

TFs dwell time analysis

The lifetime of the TFs in each cell was computed using two-component exponential decay curves as the following equation [67]:

$$F(t) = f_1 e^{-t/\tau s} + (1- f_1)e^{-t/\tau ns}$$

The lifetime was adjusted by the bleach rate (BR) as the following equation:

$$t = (BR-1)/(BR/(\max(\tau_s, \tau_{ns})-1)$$

BR was computed by taking the inverse of the average intensity decay rate (I_{DR}) [10]:

$$BR = 1/I_{DR}$$

I_{DR} was computed as the following equation:

$$I_{DR} =[(I_0-I_B)-(I_{1000}-I_B)]/(0.5 * 1000)$$

Where I_0 is the intensity at the first frame, IB is the background intensity, I_{1000} is the intensity after a thousand frames.

TFs occupancy analysis

Fluorescent molecules were identified using a custom-written MATLAB implementation of the MTT algorithm. The parameters used in the pipeline were: localisation error: 10-6.5, emission wavelength: 580 nm, exposure time: 500 ms, number of deflation loops: 0, number of maximum expected diffusion constant: 0.2 $\mu m^2/s$, number of gaps allowed: 1, point scale factor scaling: 1.35, detection box size: 9, minimum intensity: 0, maximum optimisation iteration: 50, position tolerance: 1.5, search exploration factor: 1.2, number of past frames data used in trajectories: 10, maximum trajectories competitors: 3, intensity probability weighting: 0.9 and diffusion probability weighting: 0.5. The intensity decay due to photobleaching was corrected during the TFs occupancy analysis.

GFP/RFP spots were detected by the signal intensity. The intensity of acquired images was segmented using Otsu's method. The pixels with the highest few segments were grouped into blobs based on their connectivity. The detected GFP and RFP signal was filtered by the pixel size (less than 10% of the image size).

On-state was defined when the post-aligned RFP signal appeared within the 4-pixel radius of the GFP signal. SOX2 was defined as colocalised with the GFP signal when appeared within the 4-pixel radius region. The GFP signal was detected in each acquired frame and used as a reference for the region of interest (4-pixel radius) in the subsequent frame for detecting RFP and SOX2 co-localisation.

Locus mobility analysis

For locus mobility analysis, SNAP-tag SOX2 KI mESCs were plated into an 8-well chambered dish and cultured in 2i medium for 2 h. Then, mESCs were cultured in the imaging 2i medium for live imaging as described in the "Live cell imaging" subsection. The acquired images were processed through the customised MATLAB pipeline for GFP and SOX2 detection in each frame. The movement of detectable GFP spots (in pixels) between adjacent frames was recorded. The mean locus mobility changes with or without SOX2 binding events were calculated in each cell.

Dual HILO imaging

HaloTag-hSOX2 KI mESCs (5×10^4) were transferred onto a laminin 511-coated 8-well chambered dish and cultured in 2i medium for 2 h. Then, cells were incubated with JF_{549}-Halo-Tag ligand (5 nM, LAVIS LAB, Ashburn, USA, NF-1-183) and with JF_{646}-Halo-Tag ligand (250 nM, LAVIS LAB, Ashburn, USA, NF-1-005) dissolved in imaging 2i medium for 30 min at 37°C and 5% CO_2 in the dark. The excess Halo-Tag ligand was removed by washing the cells 3 times with the imaging 2i medium. Cells were imaged in the 2i medium containing VectaCell Trolox Antifade Reagent and Hoechst33342.

Time-lapses were acquired using a Nikon H-TIRF microscope (Nikon Instruments Inc.), a 100× 1.49 NA Oil Nikon Apo TIRF objective (Nikon Instruments Inc.) and two Sona sCMOS cameras (Andor Technology, Oxford Instruments, Belfast, UK). The emission signal was split using a TuCam adapter (Andor Technology, Oxford Instruments, Belfast, UK) with an 'FF640, 579/34-25, 679/41-25' filter cube. The instrument was controlled by the Nikon NIS-Elements software (Laboratory Imaging s.r.o.,

Praha, Czech Republic). Dual HILO SMT imaging was performed simultaneously using a 560 nm laser line and a 640 nm laser line with a TRF89902-NK TIRF ET quad band filter cube (Chroma Technology Corp, Bellow Falls, VT, USA). The microscopy was set up for HILO image acquisition for slow tracking of fluorescent molecules (150 frames, 500 ms camera exposure, no interval time).

TFs cluster analysis

Fluorescent signal from the saturated labelling channel was quantified using a custom-written MATLAB pipeline. The high-, medium- and low- intensity regions in each nucleus were defined based on fluorescent signal intensity (the pixels with highest 8% signal as high-intensity region, the following 30% as medium-intensity region and the rest as low-intensity region). The single molecule detection, as described in the "TFs occupancy analysis" subsection, was performed for the sparse labelling channel within various ROIs with a radius of 4 pixels (440 nm), selected from the high-intensity regions. The overlap analysis between sparse and saturated labelling channels were performed using the customised MATLAB pipeline.

Capture-C Extraction

Nuclei containing chromatin were isolated and fixed as detailed previously [68,69]. Briefly, 10 x 10^6 mouse embryonic stem cells E14 (donation from Rob Klose lab) were trypsinised and collected in 50ml falcon tubes in 9.3 ml medium (Dulbecco's Modified Eagle Medium supplemented with 15% fetal bovine serum, 2 mM GlutaMAX, 0.5 mM beta-Mercaptoethanol, 1x non-essential amino acids, 1x penicillin/streptomycin solution and 10 ng/mL leukemia-inhibitory factor (produced in-house)) and crosslinked with 1.25 ml 16% formaldehyde (1.89% final, Thermo Fisher Scientific, 10751395) through rotation for 10 min at RT. Crosslinking reaction was quenched with 1.5 ml 1M cold glycine, washed with cold PBS and lysed for 20 min at 4°C in lysis buffer (10 mM Tris, 10 mM NaCl, 0.2% NP-40, cOmplete protease inhibitors [Roche, 05056489001], pH 8). Finally, cells were pelleted and

resuspended in 500 µl lysis buffer per 5 x 10^6 cells and snap frozen on dry ice. Fixed chromatin was stored at - 80°C.

Capture-C Library Preparation

Capture-C libraries were prepared as described previously [69]. Briefly, cell lysates from 5 x 10^6 cells were thawed on ice, pelleted and subsequently resuspended in 250 µl 1x DpnII buffer (New England Biolabs, B0543). Each lysate was treated with SDS (0.28% final concentration, Thermo Fisher Scientific, AM9820) through interval shaking (500 rpm, 30 sec on/off) for 1 h at 37°C, then quenched with Triton X-100 (1.67% final concentration) through interval shaking (500 rpm, 30 sec on/off). Chromatin was digested with 3 x 10 µl DpnII (homemade) through interval shaking (500 rpm, 30 sec on/off) for 24 h at 37°C. 100 µl aliquot was taken to assess the quality of digest on agarose gel upon reverse crosslinking. The remaining chromatin was ligated with 8 µl T4 Ligase (240 U, Thermo Fisher Scientific, EL0013) in a volume of 1440 µl for 22 h at 16°C. Subsequently, the nuclei containing ligated chromatin were pelleted to remove non-nuclear chromatin, reverse-crosslinked and ligated DNA was purified by phenol-chloroform extraction. The resulting DNA was resuspended in 200 µl water and sonicated for 13 cycles (30 sec on/off, Bioruptor Pico) until a fragment size of approximately 200 bp was achieved. Fragments were size selected using Ampure XP beads (selection ratios: 0.85 x / 0.4x, Beckman Coulter, A63881). 1-5 µg DNA was adaptor-ligated and indexed using the NEBNext End Repair Module (New England Biolabs, E6050), dA-Tailing (New England Biolabs, E6053), Quick Ligation modules (New England Biolabs, E6056), and NEBNext Multiplex Oligos for Illumina Primer sets 1 (New England Biolabs, E7335) and 2 (New England Biolabs, E7500S). The libraries were amplified with Herculase II Fusion Polymerase kit (Agilent, 600677) for 6 PCR cycles. The probes for hybridisation (supp Table. 1) were designed in the following manner: two capture probes (aligned to mm10, 70 bp each) were designed for each promoter-containing DpnII digest fragment using the online tool by the Hughes lab [70] with filtering parameters as follows:

Duplicates: < 2, Density < 30, SRepeatLength < 30, Duplication: FALSE. If no probes could be designed for the restriction fragment directly overlapping the TSS, the next-nearest DpnII fragment was chosen, if it was within 500 bp of the TSS.

Indexed libraries were measured with Qubit dsDNA BR Assay (Invitrogen, Q32850) and pooled by mass (1.5 µg each) prior to hybridisation. Hybridisation was performed with the pool of probes (2.9 nM each) using KAPA HyperCapture Reagent Kit (Roche, 9075828001) and KAPA HyperCapture Bead Kit (Roche, 9075798001) according to Roche protocol for 72 h followed by a 24-hour hybridisation (double capture). Quantification of captured libraries was performed via qPCR using the KAPA Sybr Fast Universal kit (KAPA, KK4602) and sequenced on Illumina NextSeq 550 (Illumina, SY-415-1002) using High-Output v2.5 Kit (75 cycles, Illumina, 20024906).

Capture-C analysis

Paired-end reads were aligned to mm10 and filtered for Hi-C artefacts using HiCUP v 0.8.3 [71] and Bowtie2 v2.3.5.1 [72], with fragment filter set to 100 - 800 bp. Read counts of reads aligning to captured gene promoters and interaction scores (significant interactions) were then called by the Bioconductor package Chicago v1.6.0 [73]. For visualisation of Capture-C data, weighted pooled read counts from Chicago data files were normalised to the total read count aligning to captured gene promoters in the sample and further to the number of promoters in the respective capture experiment. Normalised reads were then multiplied by a constant number to simplify visualisation: (normCounts = counts/cov*nprom*100000). The enrichment data for H3K4mel [74] and SOX2 [75] were obtained from previous papers.

References

1. Rodriguez, J. & Larson, D. R. Transcription in Living Cells: Molecular Mechanisms of Bursting. *Annu. Rev. Biochem.* **89**, 189–212 (2020).
2. Beckman, W. F., Jiménez, M. Á. L. & Verschure, P. J. Transcription bursting and epigenetic plasticity: an updated view. *Epigenetics Commun.* **1**, 6 (2021).
3. Gibcus, J. H. & Dekker, J. The hierarchy of the 3D genome. *Mol. Cell* **49**, 773–782 (2013).
4. Jordan Rowley, M. & Corces, V. G. Organizational Principles of 3D Genome Architecture. *Nat. Rev. Genet.* **19**, 789–800 (2018).
5. Miron, E. *et al.* Chromatin arranges in chains of mesoscale domains with nanoscale functional topography independent of cohesin. *Sci. Adv.* **6**, eaba8811 (2020).
6. Tokunaga, M., Imamoto, N. & Sakata-Sogawa, K. Highly inclined thin illumination enables clear single-molecule imaging in cells. *Nat. Methods* **5**, 159–161 (2008).
7. Mortensen, K. I., Churchman, L. S., Spudich, J. A. & Flyvbjerg, H. Optimized localization analysis for single-molecule tracking and super-resolution microscopy. *Nat. Methods* **7**, 377–381 (2010).
8. Izeddin, I. *et al.* Single-molecule tracking in live cells reveals distinct target-search strategies of transcription factors in the nucleus. *eLife* **3**, e02230 (2014).
9. Liu, Z., Lavis, L. D. & Betzig, E. Imaging Live-Cell Dynamics and Structure at the Single-Molecule Level. *Mol. Cell* **58**, 644–659 (2015).
10. Chen, J. *et al.* Single-Molecule Dynamics of Enhanceosome Assembly in Embryonic Stem Cells. *Cell* **156**, 1274–1285 (2014).
11. White, M. D. *et al.* Long-Lived Binding of Sox2 to DNA Predicts Cell Fate in the Four-Cell Mouse Embryo. *Cell* **165**, 75–87 (2016).

12. Dahal, L., Walther, N., Tjian, R., Darzacq, X. & Graham, T. G. W. Single-molecule tracking (SMT): a window into live-cell transcription biochemistry. *Biochem. Soc. Trans.* **51**, 557–569 (2023).

13. Ochiai, H., Sugawara, T., Sakuma, T. & Yamamoto, T. Stochastic promoter activation affects Nanog expression variability in mouse embryonic stem cells. *Sci. Rep.* **4**, 7125 (2014).

14. Boer, B. *et al.* Elevating the levels of Sox2 in embryonal carcinoma cells and embryonic stem cells inhibits the expression of Sox2:Oct-3/4 target genes†. *Nucleic Acids Res.* **35**, 1773–1786 (2007).

15. Masui, S. *et al.* Pluripotency governed by Sox2 via regulation of Oct3/4 expression in mouse embryonic stem cells. *Nat. Cell Biol.* **9**, 625–635 (2007).

16. Fong, H., Hohenstein, K. A. & Donovan, P. J. Regulation of Self-Renewal and Pluripotency by Sox2 in Human Embryonic Stem Cells. *Stem Cells* **26**, 1931–1938 (2008).

17. Kopp, J. L., Ormsbee, B. D., Desler, M. & Rizzino, A. Small increases in the level of Sox2 trigger the differentiation of mouse embryonic stem cells. *Stem Cells Dayt. Ohio* **26**, 903–911 (2008).

18. Zhang, S. & Cui, W. Sox2, a key factor in the regulation of pluripotency and neural differentiation. *World J. Stem Cells* **6**, 305–311 (2014).

19. Ohishi, H. *et al.* STREAMING-tag system reveals spatiotemporal relationships between transcriptional regulatory factors and transcriptional activity. *Nat. Commun.* **13**, 7672 (2022).

20. Li, J. *et al.* Single-Molecule Nanoscopy Elucidates RNA Polymerase II Transcription at Single Genes in Live Cells. *Cell* **178**, 491-506.e28 (2019).

21. Li, J. *et al.* Single-gene imaging links genome topology, promoter–enhancer communication and transcription control. *Nat. Struct. Mol. Biol.* **27**, 1032–1040 (2020).

22. Tome, J. M., Tippens, N. D. & Lis, J. T. Single-molecule nascent RNA sequencing identifies regulatory domain architecture at promoters and enhancers. *Nat. Genet.* **50**, 1533–1541 (2018).

23. Chen, F. X., Smith, E. R. & Shilatifard, A. Born to run: control of transcription elongation by RNA polymerase II. *Nat. Rev. Mol. Cell Biol.* **19**, 464–478 (2018).

24. Core, L. & Adelman, K. Promoter-proximal pausing of RNA polymerase II: a nexus of gene regulation. *Genes Dev.* **33**, 960–982 (2019).

25. Rodda, D. J. *et al.* Transcriptional Regulation of *Nanog* by OCT4 and SOX2*. *J. Biol. Chem.* **280**, 24731–24737 (2005).

26. Agrawal, P. *et al.* Genome editing demonstrates that the −5 kb Nanog enhancer regulates Nanog expression by modulating RNAPII initiation and/or recruitment. *J. Biol. Chem.* **296**, 100189 (2021).

27. Cho, W.-K. *et al.* Mediator and RNA polymerase II clusters associate in transcription-dependent condensates. *Science* **361**, 412–415 (2018).

28. Holmes, Z. E. *et al.* The Sox2 transcription factor binds RNA. *Nat. Commun.* **11**, 1805 (2020).

29. Hou, L. *et al.* Concurrent binding to DNA and RNA facilitates the pluripotency reprogramming activity of Sox2. *Nucleic Acids Res.* **48**, 3869–3887 (2020).

30. de Jonge, W. J., Patel, H. P., Meeussen, J. V. W. & Lenstra, T. L. Following the tracks: How transcription factor binding dynamics control transcription. *Biophys. J.* **121**, 1583–1592 (2022).

31. Métivier, R., Reid, G. & Gannon, F. Transcription in four dimensions: nuclear receptor-directed initiation of gene expression. *EMBO Rep.* **7**, 161–167 (2006).

32. Pedraza, J. M. & Paulsson, J. Effects of Molecular Memory and Bursting on Fluctuations in Gene Expression. *Science* **319**, 339–343 (2008).

33. Wang, Y., Liu, F., Li, J. & Wang, W. Reconciling the concurrent fast and slow cycling of proteins on gene promoters. *J. R. Soc. Interface* **11**, 20140253 (2014).

34. Wang, Y., Ni, T., Wang, W. & Liu, F. Gene transcription in bursting: a unified mode for realizing accuracy and stochasticity. *Biol. Rev.* **94**, 248–258 (2019).

35. Liu, Z. *et al.* 3D imaging of Sox2 enhancer clusters in embryonic stem cells. *eLife* **3**, e04236 (2014).

36. Ochiai, H., Sugawara, T. & Yamamoto, T. Simultaneous live imaging of the transcription and nuclear position of specific genes. *Nucleic Acids Res.* **43**, e127 (2015).

37. Platania, A. *et al.* Competition between transcription and loop extrusion modulates promoter and enhancer dynamics. 2023.04.25.538222 Preprint at https://doi.org/10.1101/2023.04.25.538222 (2023).

38. Oksuz, O. *et al.* Transcription factors interact with RNA to regulate genes. *Mol. Cell* **83**, 2449-2463.e13 (2023).

39. Arnold, P. R., Wells, A. D. & Li, X. C. Diversity and Emerging Roles of Enhancer RNA in Regulation of Gene Expression and Cell Fate. *Front. Cell Dev. Biol.* **7**, (2020).

40. Blinka, S., Reimer, M. H., Pulakanti, K. & Rao, S. Super-Enhancers at the *Nanog* Locus Differentially Regulate Neighboring Pluripotency-Associated Genes. *Cell Rep.* **17**, 19–28 (2016).

41. Blinka, S. & Rao, S. Nanog Expression in Embryonic Stem Cells - An Ideal Model System to Dissect Enhancer Function. *BioEssays News Rev. Mol. Cell. Dev. Biol.* **39**, (2017).

42. Mahat, D. B. *et al.* Single-cell nascent RNA sequencing unveils coordinated global transcription. *Nature* **631**, 216–223 (2024).

43. Das, S., Jena, S. & Levasseur, D. N. Alternative Splicing Produces Nanog Protein Variants with Different Capacities for Self-renewal and Pluripotency in Embryonic Stem Cells*. *J. Biol. Chem.* **286**, 42690–42703 (2011).

44. Hamamoto, K., Umemura, Y., Makino, S. & Fukaya, T. Dynamic interplay between non-coding enhancer transcription and gene activity in development. *Nat. Commun.* **14**, 826 (2023).

45. Lodato, M. A. *et al.* SOX2 Co-Occupies Distal Enhancer Elements with Distinct POU Factors in ESCs and NPCs to Specify Cell State. *PLOS Genet.* **9**, e1003288 (2013).

46. Pomp, W., Meeussen, J. V. & Lenstra, T. L. Transcription factor exchange enables prolonged transcriptional bursts. *Mol. Cell* **84**, 1036 (2024).

47. Stavreva, D. A. *et al.* Transcriptional Bursting and Co-bursting Regulation by Steroid Hormone Release Pattern and Transcription Factor Mobility. *Mol. Cell* **75**, 1161-1177.e11 (2019).

48. Donovan, B. T. *et al.* Live-cell imaging reveals the interplay between transcription factors, nucleosomes, and bursting. *EMBO J.* **38**, e100809 (2019).

49. Popp, A. P., Hettich, J. & Gebhardt, J. C. M. Altering transcription factor binding reveals comprehensive transcriptional kinetics of a basic gene. *Nucleic Acids Res.* **49**, 6249–6266 (2021).

50. Du, M. *et al.* Direct observation of a condensate effect on super-enhancer controlled gene bursting. *Cell* **187**, 331-344.e17 (2024).

51. Rambout, X., Dequiedt, F. & Maquat, L. E. Beyond Transcription: Roles of Transcription Factors in Pre-mRNA Splicing. *Chem. Rev.* **118**, 4339–4364 (2018).

52. Basu, S. *et al.* Live-cell three-dimensional single-molecule tracking reveals modulation of enhancer dynamics by NuRD. *Nat. Struct. Mol. Biol.* **30**, 1628–1639 (2023).

53. Mallanna, S. K. *et al.* Proteomic analysis of Sox2-associated proteins during early stages of mouse embryonic stem cell differentiation identifies Sox21 as a novel regulator of stem cell fate. *Stem Cells Dayt. Ohio* **28**, 1715–1727 (2010).

54. Wang, S. *et al.* Transient activation of autophagy via Sox2-mediated suppression of mTOR is an important early step in reprogramming to pluripotency. *Cell Stem Cell* **13**, 617–625 (2013).

55. Mazzocca, M., Colombo, E., Callegari, A. & Mazza, D. Transcription factor binding kinetics and transcriptional bursting: What do we really know? *Curr. Opin. Struct. Biol.* **71**, 239–248 (2021).

56. Kaur, G. *et al.* Probing transcription factor diffusion dynamics in the living mammalian embryo with photoactivatable fluorescence correlation spectroscopy. *Nat. Commun.* **4**, 1637 (2013).

57. Hörberg, J. & Reymer, A. Decoding the dual recognition mechanism of the glucocorticoid receptor for DNA and RNA: sequence versus shape. *Sci. Rep.* **13**, 16125 (2023).

58. Kaikkonen, M. U. *et al.* Remodeling of the Enhancer Landscape during Macrophage Activation Is Coupled to Enhancer Transcription. *Mol. Cell* **51**, 310–325 (2013).

59. Pnueli, L., Rudnizky, S., Yosefzon, Y. & Melamed, P. RNA transcribed from a distal enhancer is required for activating the chromatin at the promoter of the gonadotropin α-subunit gene. *Proc. Natl. Acad. Sci.* **112**, 4369–4374 (2015).

60. Schindelin, J. *et al.* Fiji: an open-source platform for biological-image analysis. *Nat. Methods* **9**, 676–682 (2012).

61. Stirling, D. R. *et al.* CellProfiler 4: improvements in speed, utility and usability. *BMC Bioinformatics* **22**, 433 (2021).

62. The MathWorks Inc. Optimization Toolbox. (2022).

63. Rueden, C. T. *et al.* PyImageJ: A library for integrating ImageJ and Python. *Nat. Methods* **19**, 1326–1327 (2022).

64. Stringer, C., Wang, T., Michaelos, M. & Pachitariu, M. Cellpose: a generalist algorithm for cellular segmentation. *Nat. Methods* **18**, 100–106 (2021).

65. Imbert, A. *et al.* FISH-quant v2: a scalable and modular tool for smFISH image analysis. *RNA* **28**, 786–795 (2022).

66. Scientific Volume Imaging. Huygens Localiser. (2024).

67. McCann, A. J. *et al.* A dominant-negative SOX18 mutant disrupts multiple regulatory layers essential to transcription factor activity. *Nucleic Acids Res.* **49**, 10931–10955 (2021).

68. Hughes, J. R. *et al.* Analysis of hundreds of cis-regulatory landscapes at high resolution in a single, high-throughput experiment. *Nat. Genet.* **46**, 205–212 (2014).

69. Downes, D. J. *et al.* Capture-C: a modular and flexible approach for high-resolution chromosome conformation capture. *Nat. Protoc.* **17**, 445–475 (2022).

70. Davies, J. O. J. *et al.* Multiplexed analysis of chromosome conformation at vastly improved sensitivity. *Nat. Methods* **13**, 74–80 (2016).

71. Wingett, S. W. *et al.* HiCUP: pipeline for mapping and processing Hi-C data. Preprint at https://doi.org/10.12688/f1000research.7334.1 (2015).

72. Langmead, B. & Salzberg, S. L. Fast gapped-read alignment with Bowtie 2. *Nat. Methods* **9**, 357–359 (2012).

73. Cairns, J. *et al.* CHiCAGO: robust detection of DNA looping interactions in Capture Hi-C data. *Genome Biol.* **17**, 127 (2016).

74. Feldmann, A., Dimitrova, E., Kenney, A., Lastuvkova, A. & Klose, R. J. CDK-Mediator and FBXL19 prime developmental genes for activation by promoting atypical regulatory interactions. *Nucleic Acids Res.* **48**, 2942–2955 (2020).

75. Whyte, W. A. *et al.* Master Transcription Factors and Mediator Establish Super-Enhancers at Key Cell Identity Genes. *Cell* **153**, 307–319 (2013).

Acknowledgments: We thank Sydney Microscopy and Micro-Analysis core facilities for ongoing technical support with imaging. We thank Dr Alexandros Pertsinidis and Dr Jieru Li (MSK, NY) for their valuable input and feedback on reviewing the manuscript. We thank Dr Luke Lavis Janelia Farm (Virginia Tech) for providing reagents necessary to establish the SOX2 HaloTag knock-in cell lines.

Funding:

NHMRC idea Grant (APP 2029719) (MF)

NHMRC idea Grant (APP2019904) (MF)

NSW Cardio-vascular Research Capacity Program – Senior Researcher grant (MF)

Grants-in Aid for Scientific Research from the Ministry of Education, Culture, Sports, Science, and Technology JP24H02326 (HOc)

Grants-in Aid for Scientific Research from the Ministry of Education, Culture, Sports, Science, and Technology JP22H02609 (HOc)

CREST from the Japan Science and Technology Agency to HOc (JPMJCR23N3)

NIG-JOINT 69A2024 (HOc)

NIG-JOINT 14R2024 (HOc)

Medical Research Centre Initiative for High Depth Omics, Kyushu University, Japan (HOc)

Author contributions:

Conceptualisation: HOc, MF

Methodology: HOc, BL, YW, NR, TD, HOh

Investigation: BL, MG, NR, YW, TD

Visualisation: YW, BL, MF

Funding acquisition: HOc, MF

Project administration: HOc, MF

Supervision: MF, TD

Writing – original draft: MF

Writing – review & editing: MF, BL, Hoc

Competing interests: Authors declare that they have no competing interests.

Supplementary Materials

Figs. S1 to S13

Movies S1 to S6

Figures

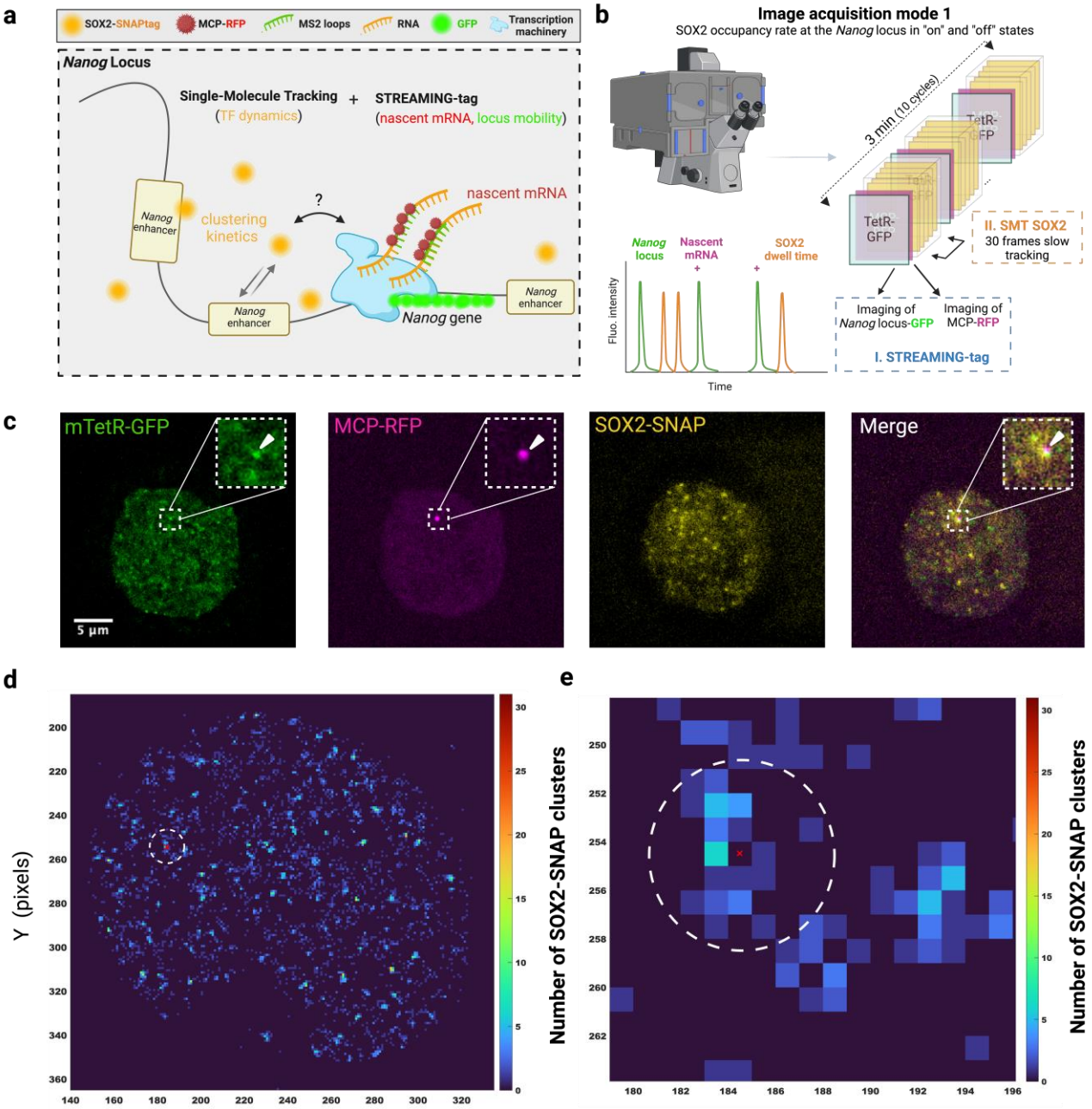

Figure 1. Multimodal imaging method to visualise transcription factor activity at a single locus resolution relative to its transcriptional state. (a) Schematic of the principle for dual imaging to capture SOX2 clustering dynamics at the *Nanog* locus relative to the event of nascent mRNA synthesis. The STREAMING-tag cassette at the *Nanog* locus enables the detection of the *Nanog* mRNA synthesis (MS2/MCP-RFP) along with the *Nanog* locus mobility (TetO/mTetR-GFP) while SNAP-tag knocked-in at the *Sox2* locus reveals chromatin occupancy rate of this TF via single

molecule tracking (SMT). (**b**) Principle of the imaging acquisition mode 1 set up to capture the fluorescent signals from STREAMING-tag and SMT detection methods in a live cell. Multimodal image acquisition uses a combination of SDC (STREAMING-tag) and HILO (SMT) microscopy (**c**) Fluorescent signals from the *Nanog* locus (mTetR-GFP), *Nanog* mRNA (MCP-RFP) and SOX2-SNAPtag. (**d**) Representative heat map of most visited locations accumulated over a 3 min period for the detected SOX2 molecules across the cell nucleus. The heat map reveals an overlap between SOX2 long dwell time and the region of interest for the *Nanog* locus (red cross). (**e**) Higher magnification of the dashed circle shown in panel **d** demonstrates SOX2 clustering activity within a 4-pixel (440 nm) radius ROI (circle dashed line) centred on the *Nanog* locus when both GFP (red cross) and RFP signals are detected.

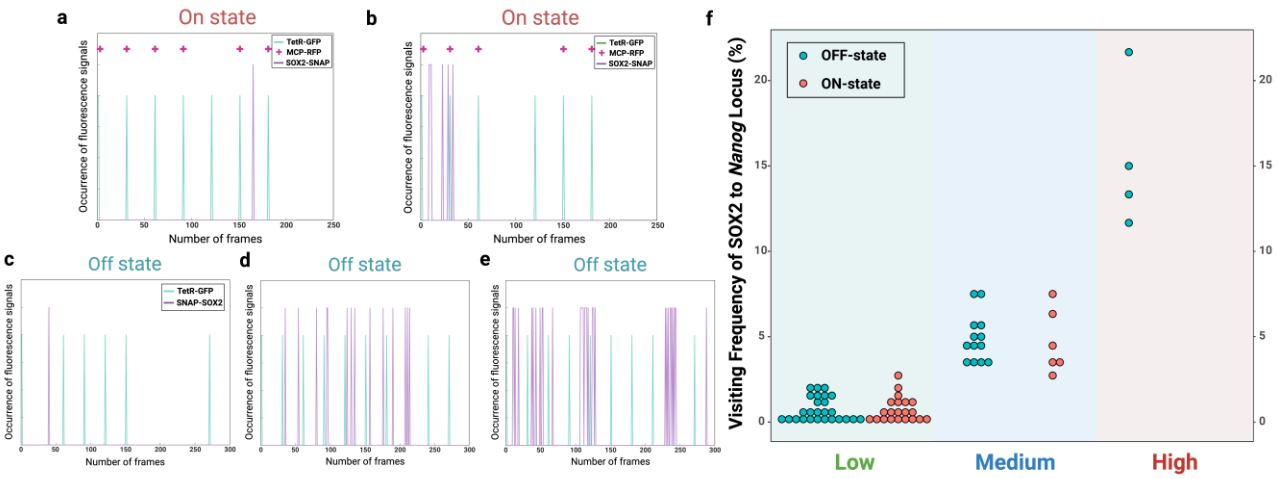

Figure 2. Multiple SOX2 clustering dynamics behaviours at the *Nanog* locus during "off" state. (**a-b**) On-state. Occurrence of fluorescence signals for GFP (green) for the *Nanog* locus, SOX2 SMT signal (purple) and RFP (magenta +) for *Nanog* transcriptional activity (on-state). **(c-e)** Off-state. Occurrence of fluorescence signals for GFP (green) for the *Nanog* locus, SOX2 SMT signal (purple) showing the visiting frequency of SOX2 when the locus is available, but production of nascent mRNA is off. **(f)** Quantitation of the different SOX2 behaviours during the on-state (n = 27) and off-state (n = 43) classified based on the visiting frequency (the total number of SOX2 molecules that have visited

this GFP positive spot normalised to the total number of frames). The visiting frequency accounts for the number of SOX2 molecules that have visited the GFP spot.

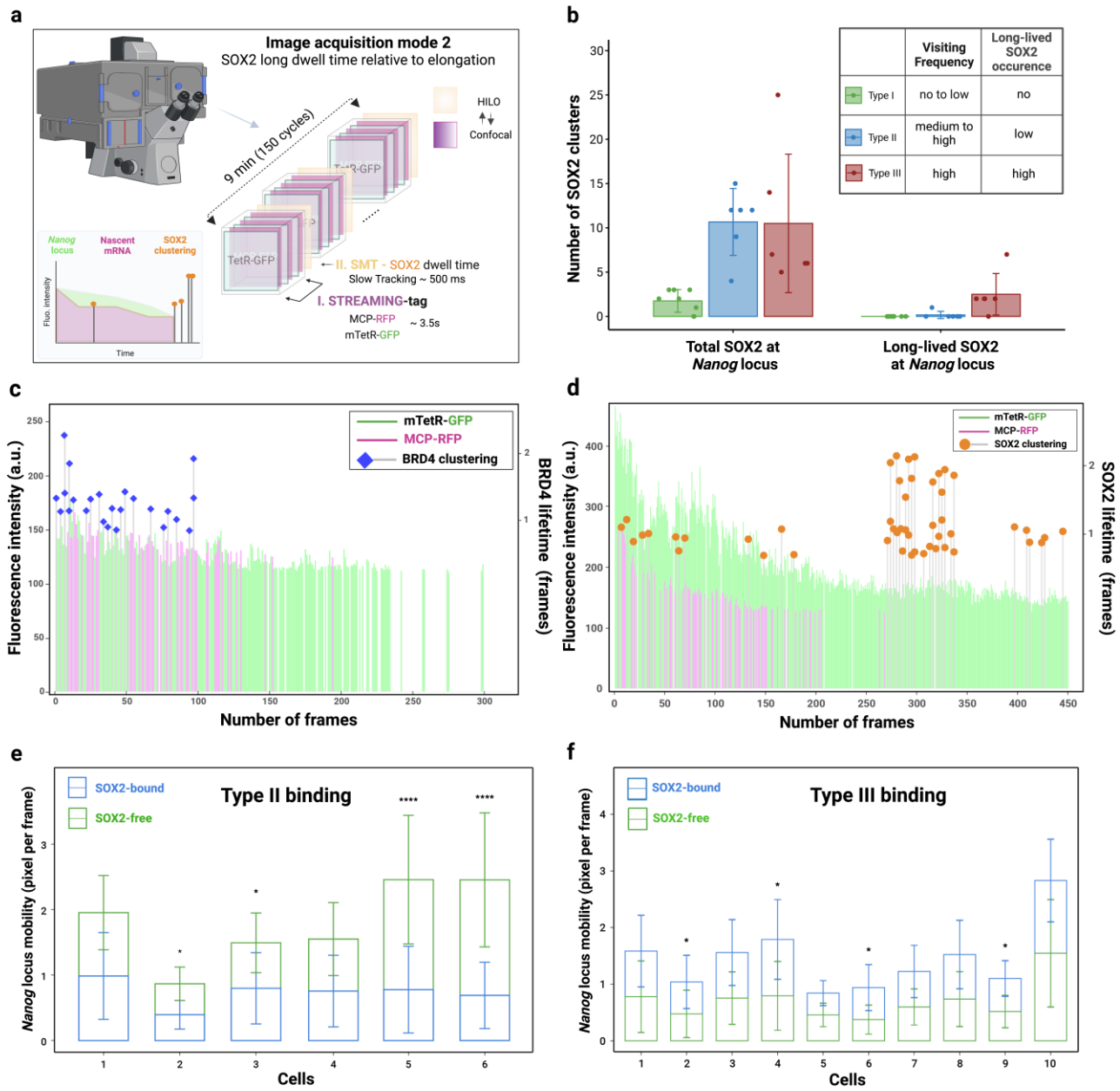

Figure 3. Distinct types of SOX2 burst dynamics associate with different locus mobility and frame the elongation process at the *Nanog* locus. (a) Image acquisition mode 2 set up to capture a full transcription cycle at the *Nanog* locus (STREAMING-tag) in parallel to SOX2 or BRD4 chromatin binding dynamics (SMT). **(b)** Quantification of detected SOX2 clusters and their relative

survival rate at the *Nanog* locus. (**c** and **d**) BRD4 **(c)** or SOX2 **(d)** dwell time relative to the elongation process. Fluorescent intensity at the *Nanog* locus is shown relative to time. *Nanog* locus signal is labelled with GFP (green), and *Nanog* mRNA synthesis (magenta). SOX2 (orange) and BRD4 (blue) long dwell times (over 2 frames) and short dwell times (over 1 frame) reveal diverse binding kinetics relative to the elongation process. (**e** and **f**) 2D *Nanog* locus mobility in the presence (blue) or absence (green) of SOX2 binding.

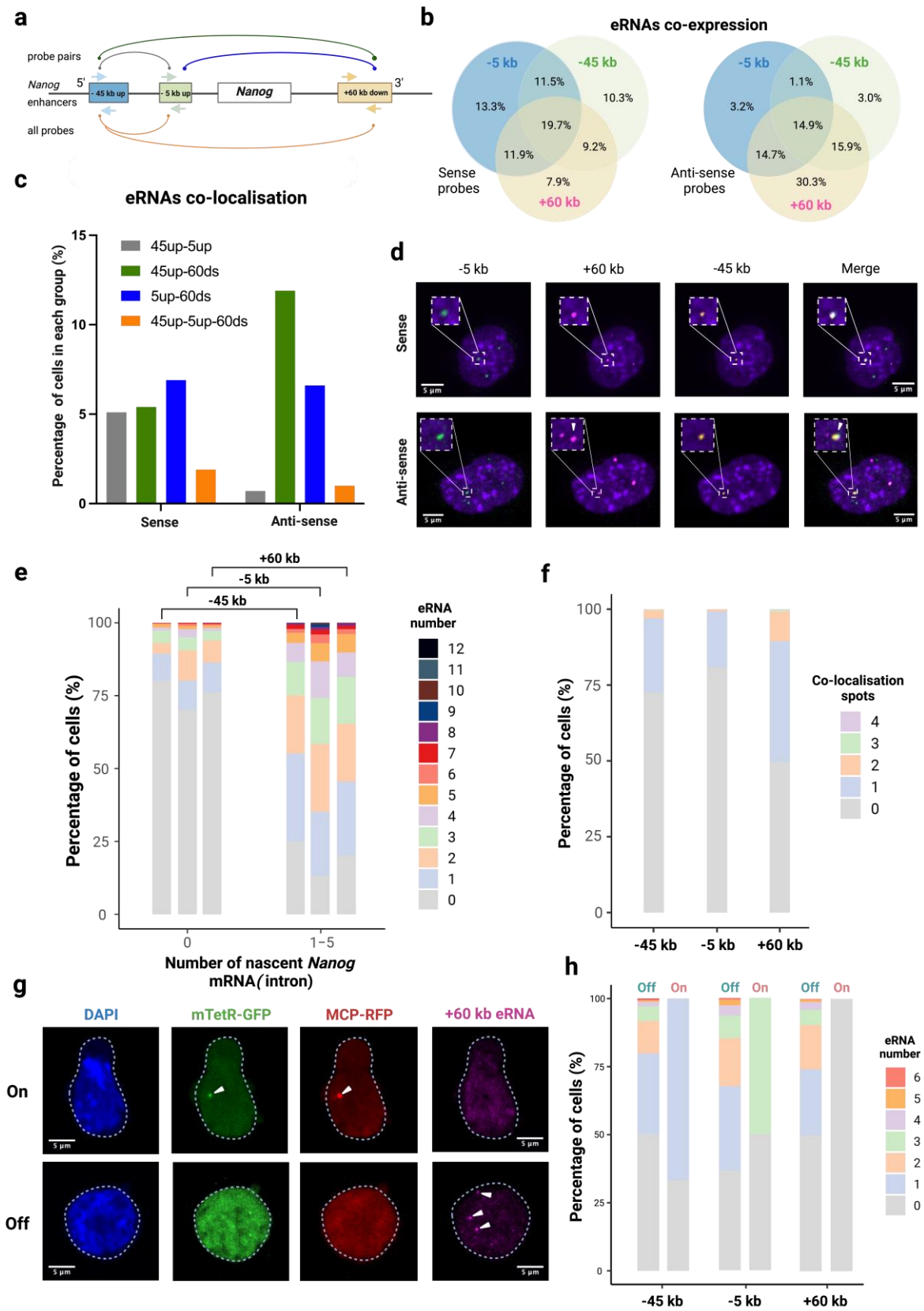

Figure 4. *Nanog* enhancers are individually or synergistically transcribed while *Nanog* nascent transcription is off. (**a**) Map of eRNAs probes (coloured arrows indicate sense and anti-sense

orientations) at three regulatory regions involved with *Nanog* gene transcription. Distances from transcription start sites are -45 kb, -5 kb and +60 kb. Coloured lines connecting the different enhancers represent the different probe combinations used to assess co-localisation: grey [-45 kb/-5 kb]; green [-45 kb/+60 kb]; blue [-5 kb/+60 kb]; orange, all three probes. (**b**) Venn diagram showing the co-expression levels of different eRNAs in embryonic stem cells. **(c)** Quantitation of three eRNAs co-localisation either assessed by pairs or in sets of three for both sense and anti-sense transcripts (≥ 4000 cells imaged per condition). **(d)** Single-molecule FISH showing sub-nuclear co-localisation of *Nanog* eRNAs for both sense and anti-sense products (green -5 kb, magenta +60 kb, -45 kb orange), scale bar 5μm. **(e)** Abundance of three different *Nanog* eRNAs correlated to the *Nanog* intron expression. **(f)** Quantitation of co-localisation events between *Nanog* eRNAs and *Nanog* intron mRNA. **(g)** Single-molecule FISH for the +60 kb eRNA combined with STREAMING tag imaging shows that the +60 kb eRNA is expressed while *Nanog* mRNA nascent transcription is off (green *Nanog* locus, red *Nanog* mRNA, magenta +60 kb eRNA, blue DAPI). **(h)** Temporal relationship between individual eRNAs from three different *Nanog* enhancers relative to the co-expression of the *Nanog* STREAMING tag reporter system.

Extended data

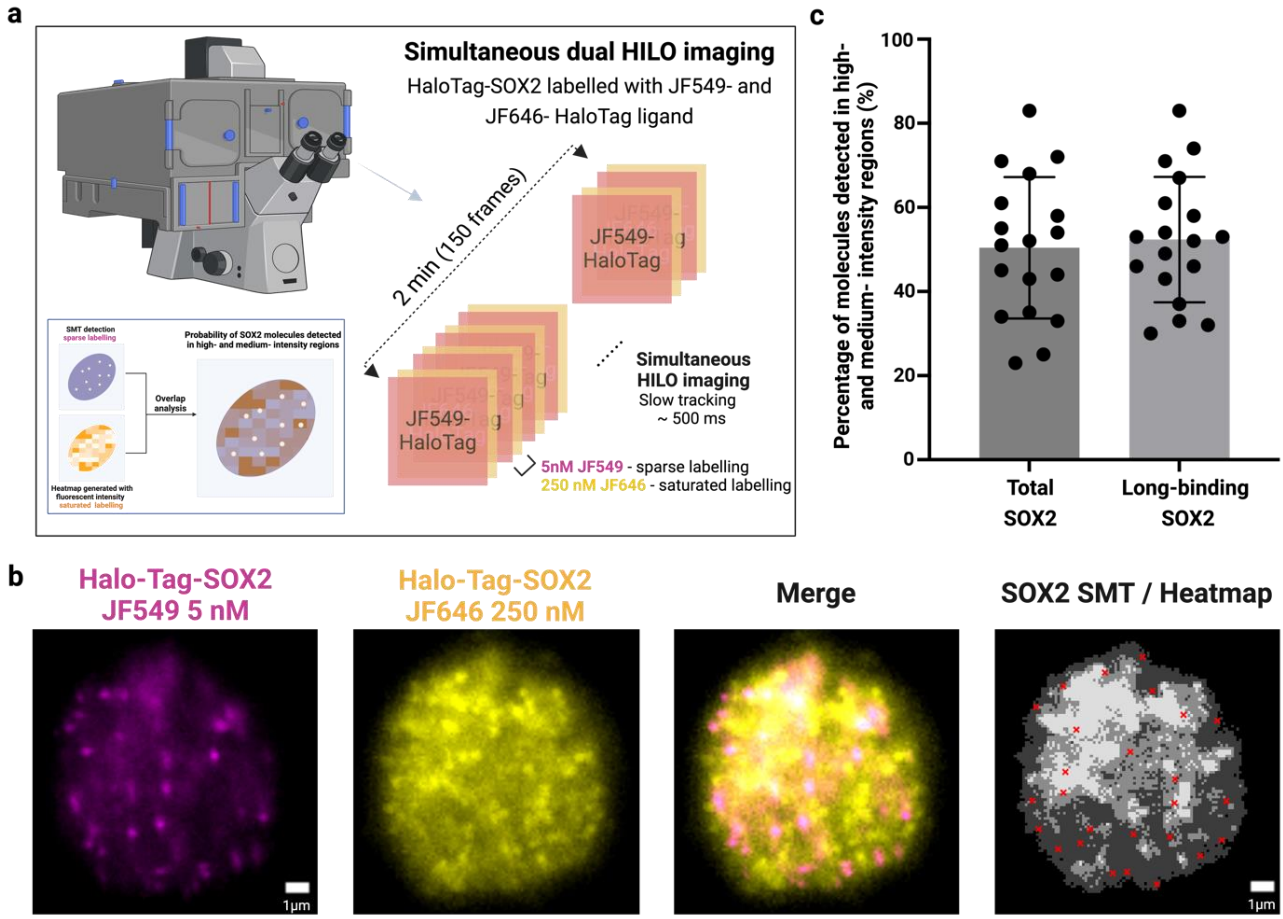

Supplementary Fig 1. Simultaneous dual-colour HILO imaging to assess SOX2 clustering events. (a) Simultaneous SMT imaging of sparse labelling HaloTag-SOX2 (JF549, magenta) and saturated labelling HaloTag-SOX2 (JF646, yellow). The saturated signal is used to define a SOX2 heatmap of low, medium and high fluorescent intensity. This heatmap is then overlaid to SOX2 SMT signal to determine occupancy kinetics. **(b)** Fluorescent signals from HaloTag-SOX2 with sparse labelling (magenta) and saturated labelling (yellow). The merged image displays the combined signals from both channels. The greyscale image shows the SMT-SOX2 detected events overlaid onto the corresponding heatmap signal, with white representing high-intensity regions (top 8%), light grey as medium-intensity (top 30%), and dark grey as low-intensity (remaining 62%). **(c)** Percentage of total SOX2 and long-dwell time events detected by SMT (JF549) and overlapped with the high- and medium- intensity regions.

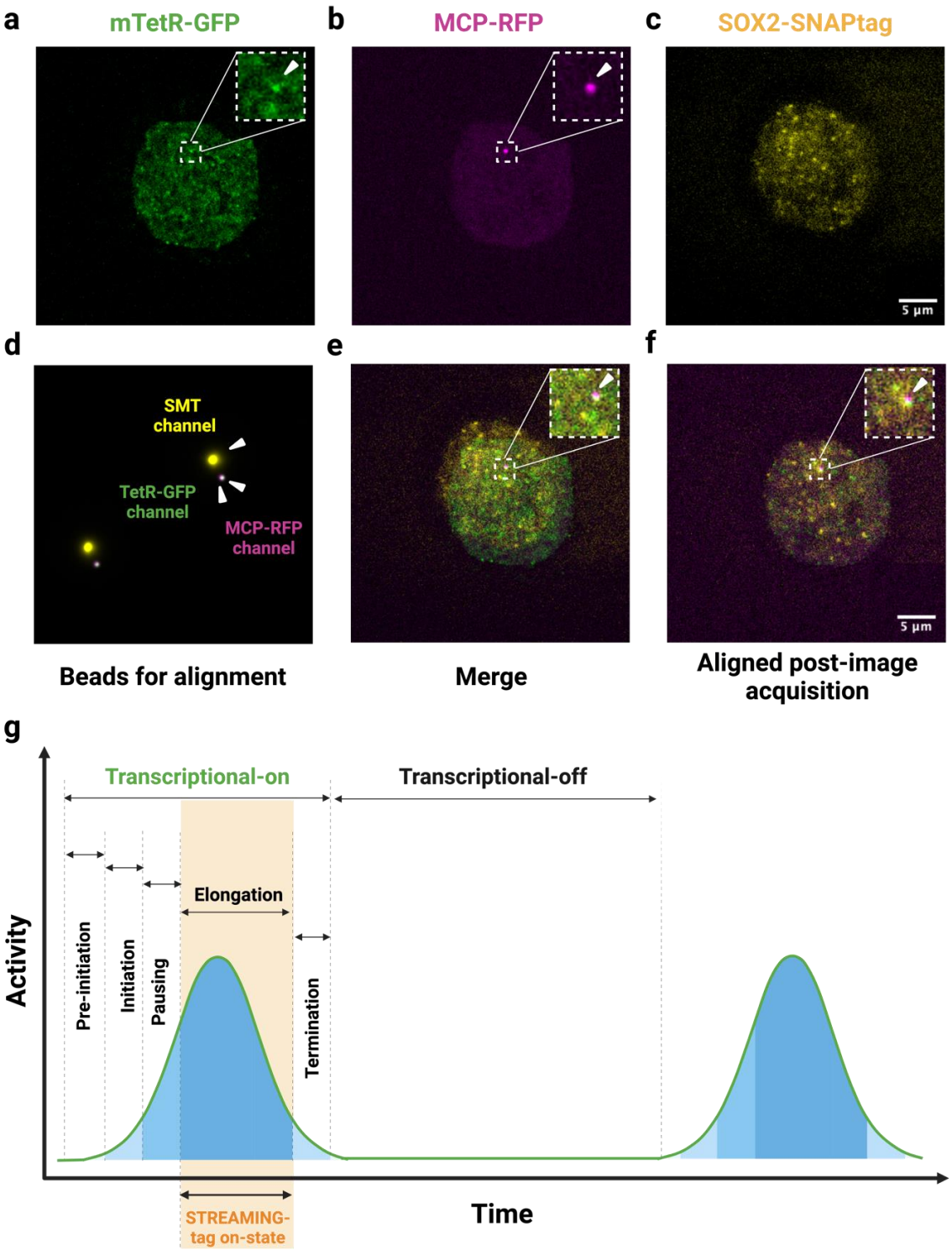

Supplementary Fig 2. Observation of SOX2 occupancy at the *Nanog* locus in relation to its transcriptional state using a combination of SDC (STREAMING-tag) and HILO (SMT) microscopy. (a-c) Alignment of multimodal imaging for live cell imaging using a combination of SDC (STREAMING-tag) and HILO (SMT) microscopy. Simultaneous imaging of the *Nanog* locus (GFP, green), *Nanog* mRNA (RFP, magenta) and SOX2-SNAP SMT (yellow). White arrowheads indicate locations where MCP-RFP and mTetR-GFP spots were observed at the same time. **(d)** Fluorescent signal from the beads was obtained using the same setup in the GFP, RFP, and SMT channels. **(e)** Merged signal of GFP, RFP and SMT channels. **(f)** The signals from GFP, RFP, and

SMT channels were merged, with spatial alignments achieved using fluorescent beads as a reference. **(g)** The STREAMING-tag reporter system (orange) is a faithful reporter of the elongation step.

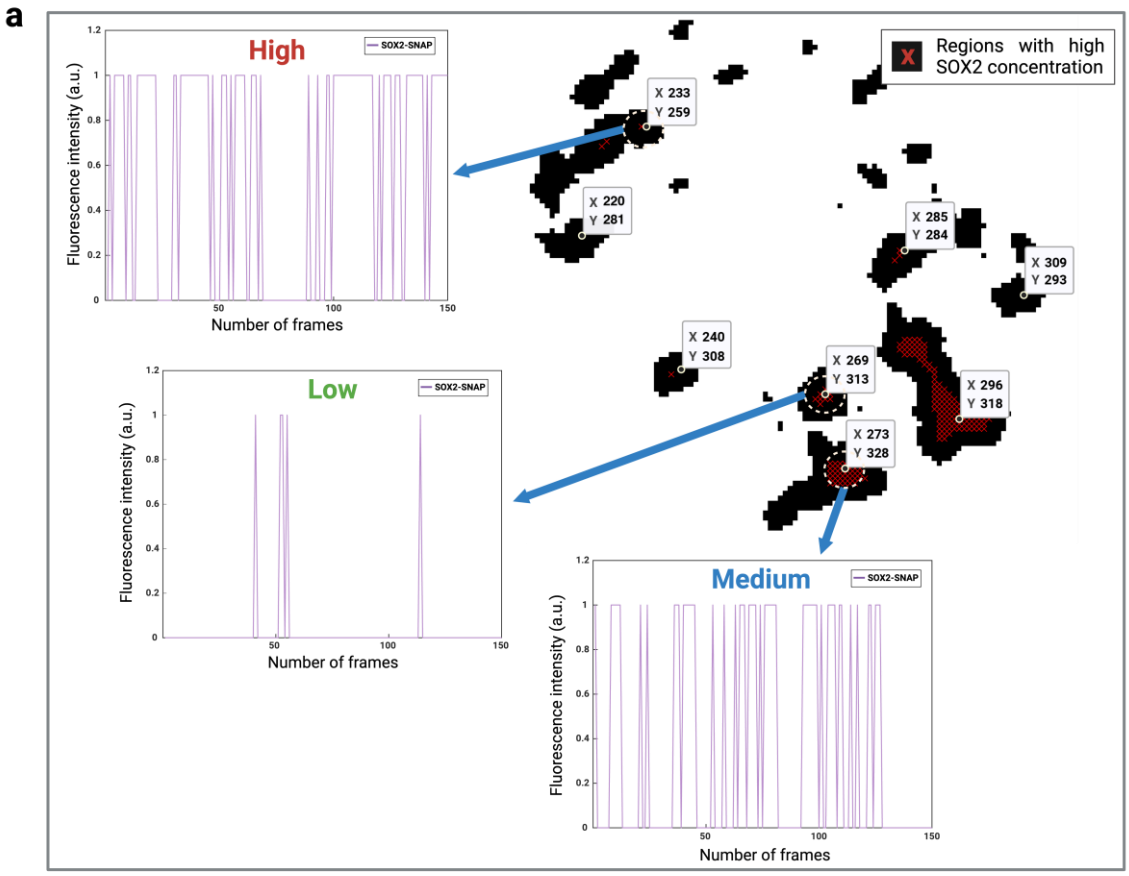

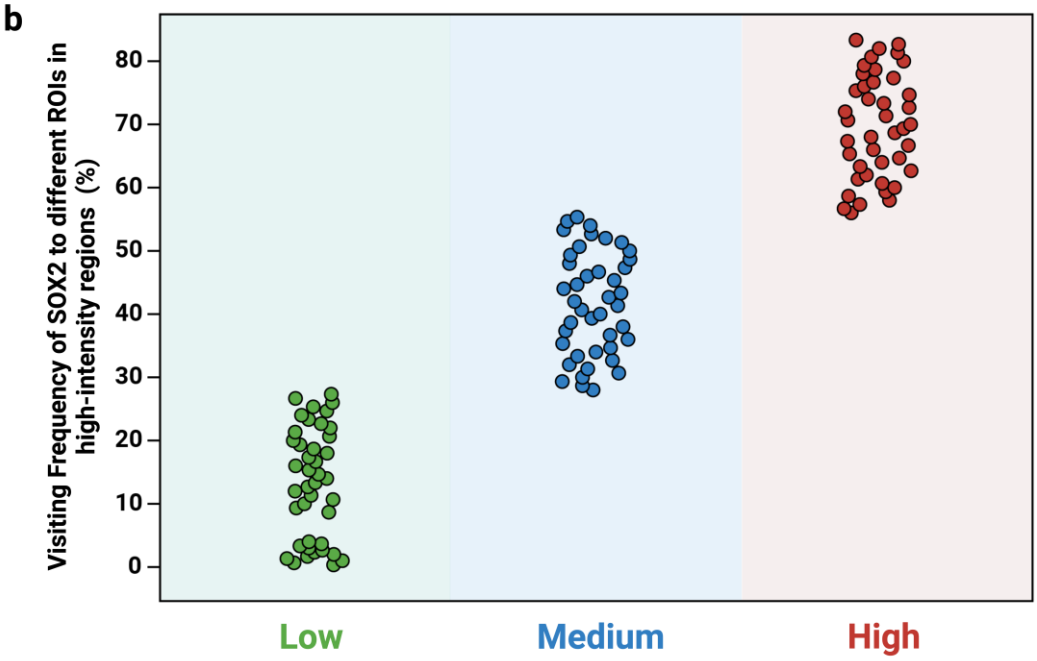

Supplementary Fig 3. Dual-colour HILO imaging analysis to assess SOX2 clustering behaviours at high-intensity regions. (a) Representative images showing the frequency of SOX2 clusters (purple) tracked over a 2-minute window across different ROIs in high-intensity regions. The

dashed circles indicate three representative ROIs with a radius of 4 pixels (440 nm). **(b)** Quantitation of different SOX2 behaviours classified based on the visiting frequency. Data represent n = 125 ROIs from 18 nuclei.

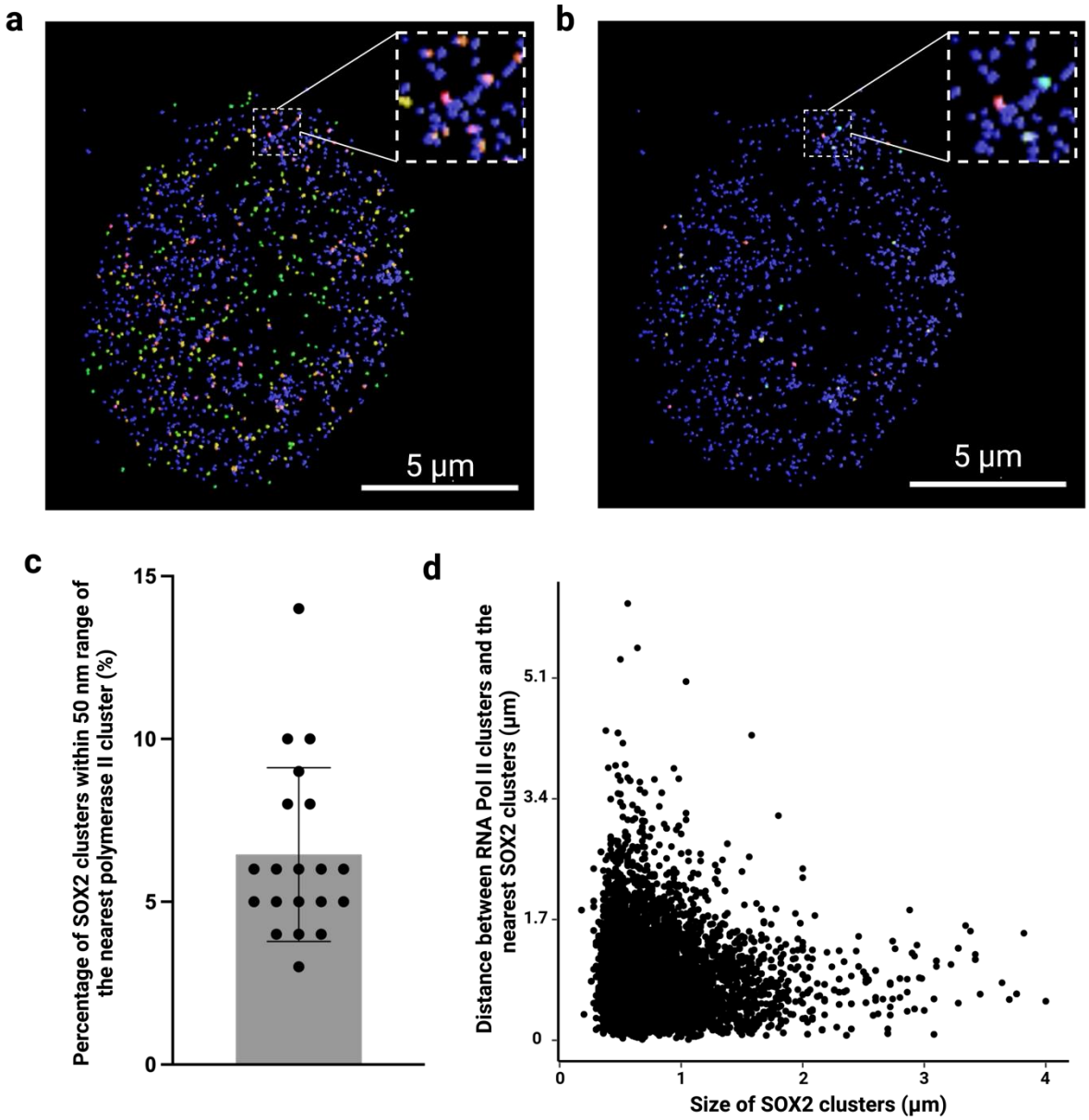

Supplementary Fig 4. Snapshot analysis of SOX2 temporal dynamics using super-resolution imaging. (a) 2D dSTORM image of active RNA polymerase II clusters (blue) and HaloTag-SOX2 clusters (colour map related to cluster distance). The colour map reflects the distance of SOX2 clusters from the nearest polymerase II cluster (green closest, and red farther). **(b)** A discreet subset of SOX2 clusters is within a 50 nm radius of the nearest RNA polymerase II cluster. **(c)** Quantification of the proportion of SOX2 clusters within 50 nm range of the nearest polymerase II cluster reveals that the vast majority of SOX2 does not co-localise with active RNA Pol II (n = 20 cells). **(d)** Correlation between the size of SOX2 clusters and the distance to the nearest RNA Pol II clusters.

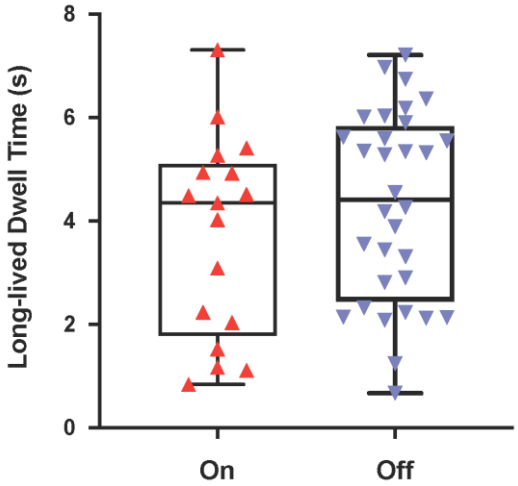

Supplementary Fig 5. Quantification of SNAP-tagged SOX2 average population long-lived dwell time while the *Nanog* locus is active. Bar chart showing the mean value of SNAP-tagged SOX2 whole nucleus population long-lived dwell time during transcriptional on- and off-states of the *Nanog* locus.

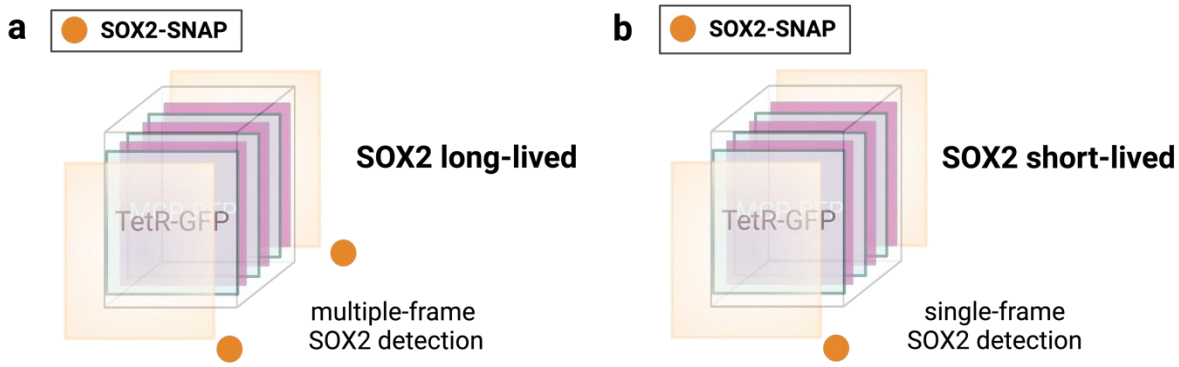

Supplementary Fig 6. Co-detection of SOX2 clustering with *Nanog* mRNA elongation. (a and b) Schematic of SOX2 long-lived (**a**, 2 frames) and short short-lived binding events (**b**, 1 frame).

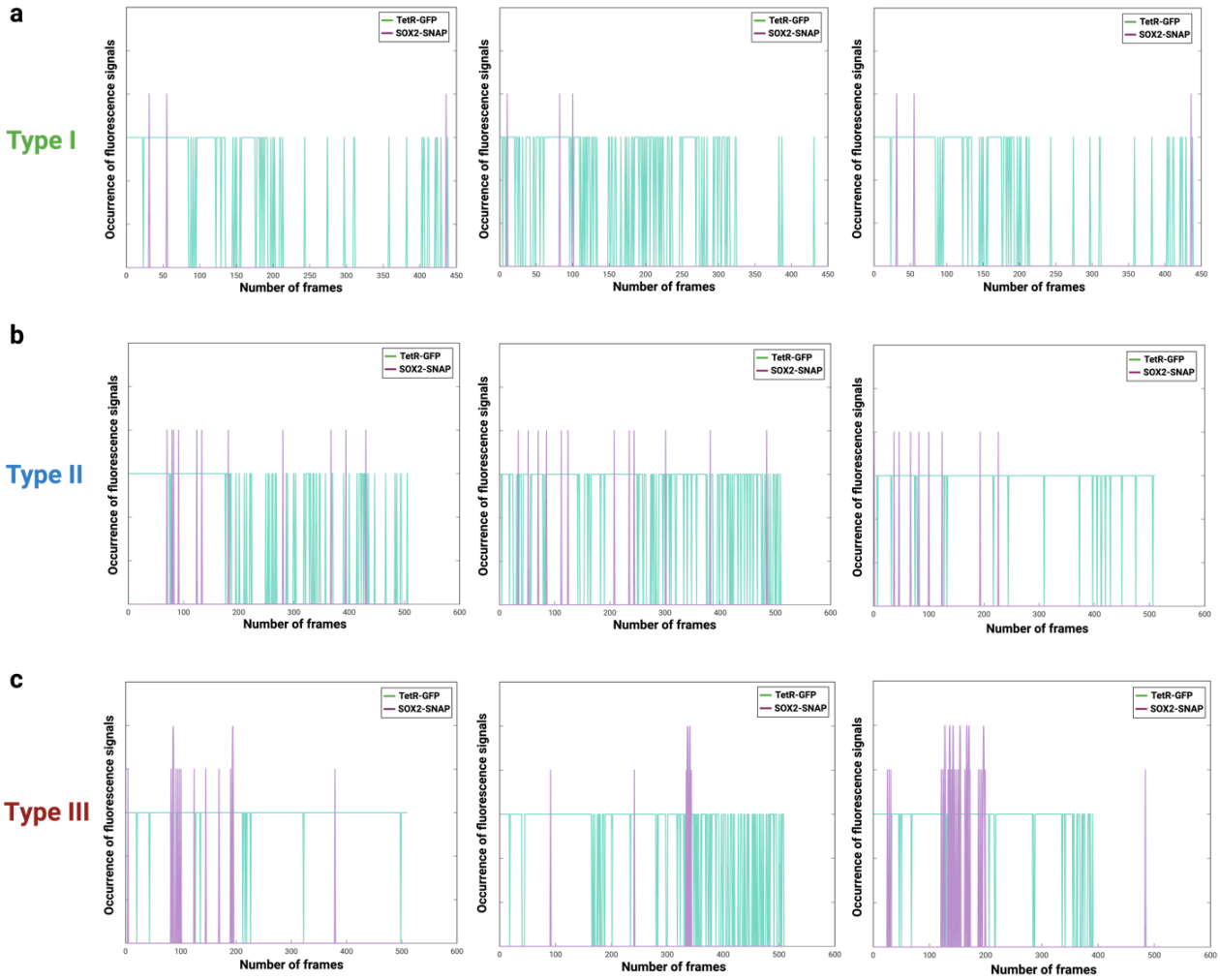

Supplementary Fig 7. SOX2 visiting frequencies at the *Nanog* locus during off-state over 9 minutes (image acquisition mode 2). (a-c) Type I **(a),** Type II **(b)** and Type III **(c)** visiting frequencies represent SOX2 clustering dynamics (purple) during the off-state (GFP) within ROIs. Short peaks (purple) represent SOX2 short-lived binding events, while high peaks (purple) in **c** indicate SOX2 long-lived binding events. The visiting frequency accounts for the number of SOX2 detected molecules that have visited the GFP spot while *Nanog* transcriptional elongation is off.

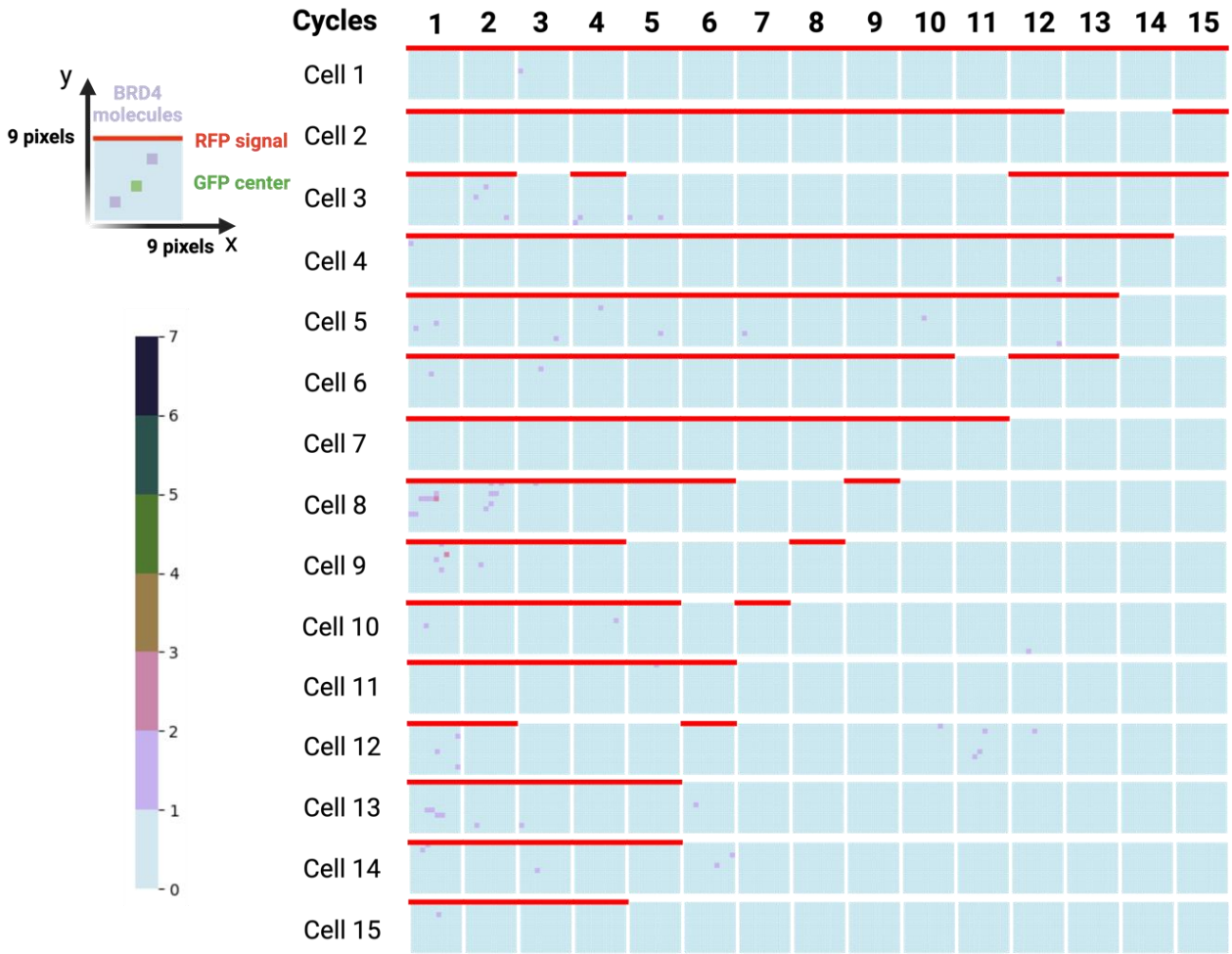

Supplementary Fig 8. BRD4 clustering behaviour during the elongation process at the *Nanog* locus in live mESC. Each row represents an individual cell across a 9-minute time window (n = 15)**.** Square plot showing BRD4 clustering behaviour during *Nanog* transcription on-state for 15 imaging cycles (9 min, 1 cycle = 10 frames) in live mESC. The heat map shows the number of BRD4 detected molecules. Each ROI (9 x 9 pixels, with a pixel size of 110 nm) has the GFP signal (*Nanog* locus) in the centre, the RFP signal (*Nanog* mRNA) is shown as a red line and the BRD4 SMT signal as a pink square. This plot summarises BRD4 visiting frequency during mRNA synthesis (on-state). Square plotting showing BRD4 clustering behaviour during *Nanog* transcription on-state for 10 imaging cycles (9 min) in mESC population (n = 15).

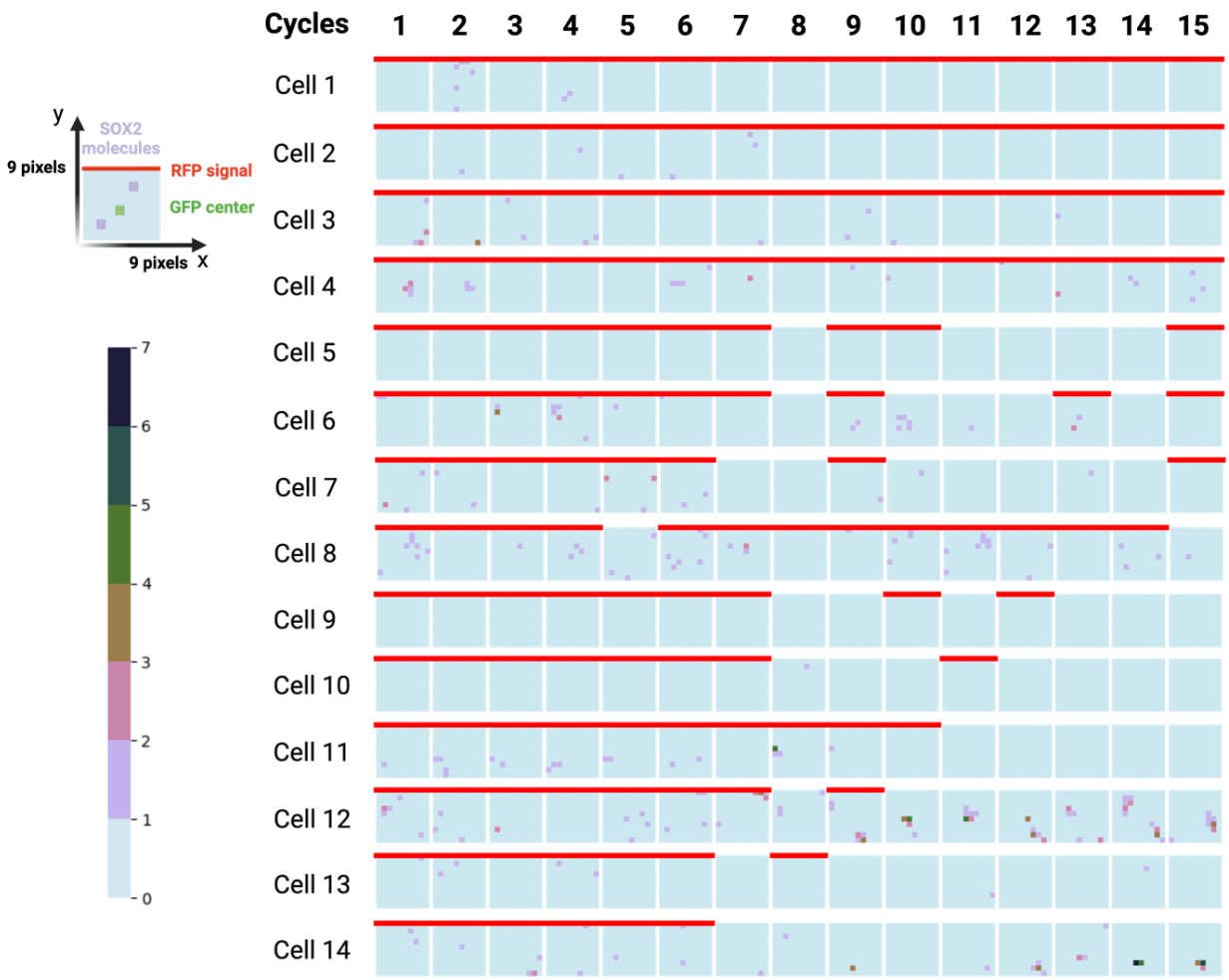

Supplementary Fig 9. SOX2 clustering behaviour during elongation process at the *Nanog* locus in mESC population. Each row represents an individual cell across a 9-minute time window (n=14). Square plot showing SOX2 clustering dynamics during *Nanog* transcription on-state for 15 imaging cycles (9 min, 1 cycle = 10 frames) in live mESC. The heat map shows the number of SOX2 detected molecules. Each ROI (9 x 9 pixels, with a pixel size of 110 nm) has the GFP signal (*Nanog* locus) in the centre, the RFP signal (*Nanog* mRNA) is shown as a red line and the SOX2 SMT signal as a pink square.

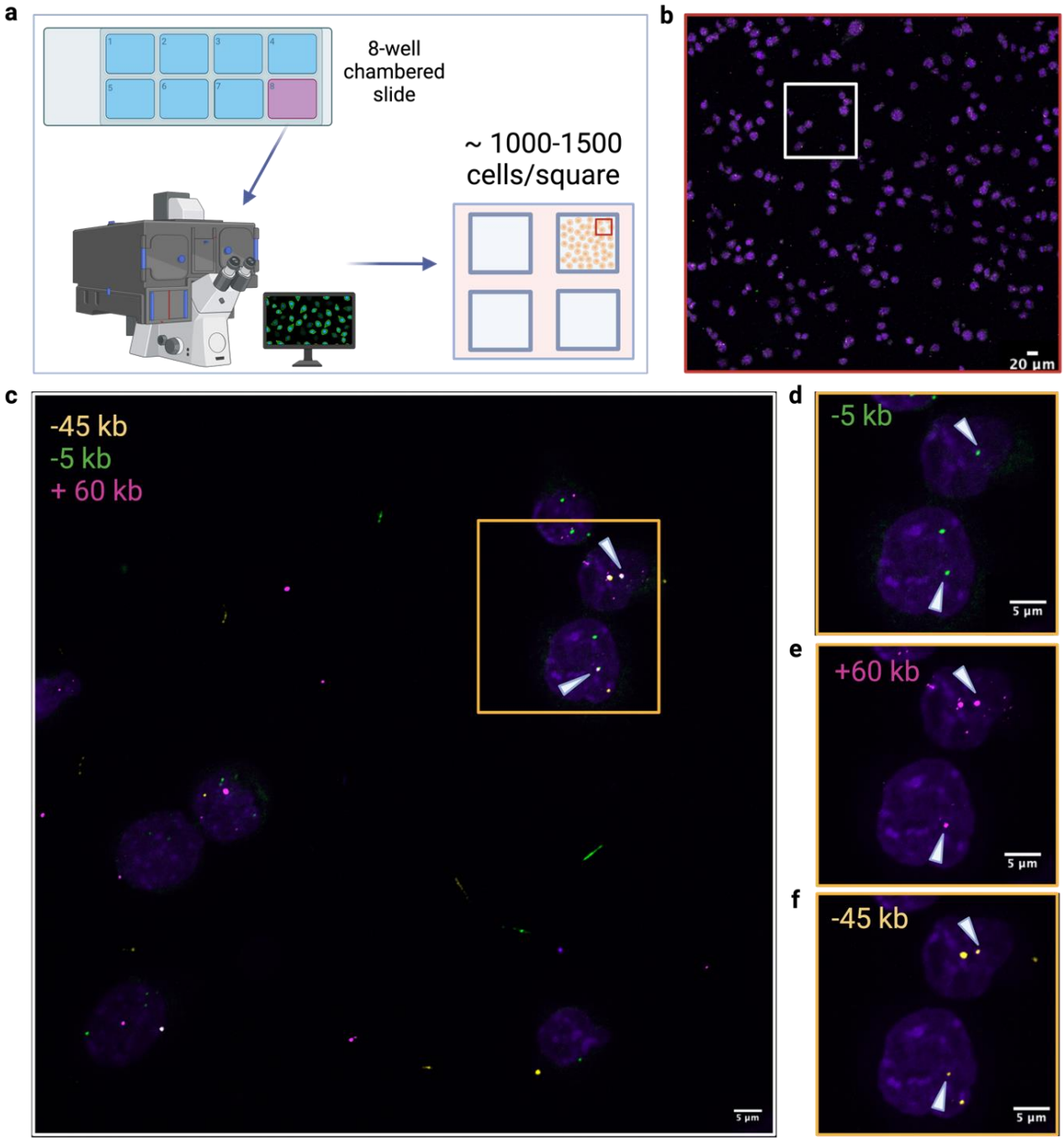

Supplementary Fig 10. Sample images used for the quantification of *Nanog* sense eRNAs co-expression and co-localisation in mESCs population. (a) Schematic of the large-scale imaging acquisition setup to capture four regions of signal from one 8-well chambered slide (around 4000-6000 cells imaged per condition). **(b)** Microscope image showing the fluorescent signal captured from a portion of the whole cell population (circled in red in suppl fig 2a). **(c)** Zoomed-in image with the fluorescent signal of -45 kb (yellow), -5 kb (green) and +60 kb (magenta) eRNAs. White arrowheads indicate locations where all 3 eRNAs were observed colocalised. **(d-f)** Zoomed-in images with the fluorescent signal of 3 eRNAs respectively, **(d)** -5 kb (green), **(e)** +60 kb (magenta) and **(f)** -45 kb (yellow), scale bar 5µm.

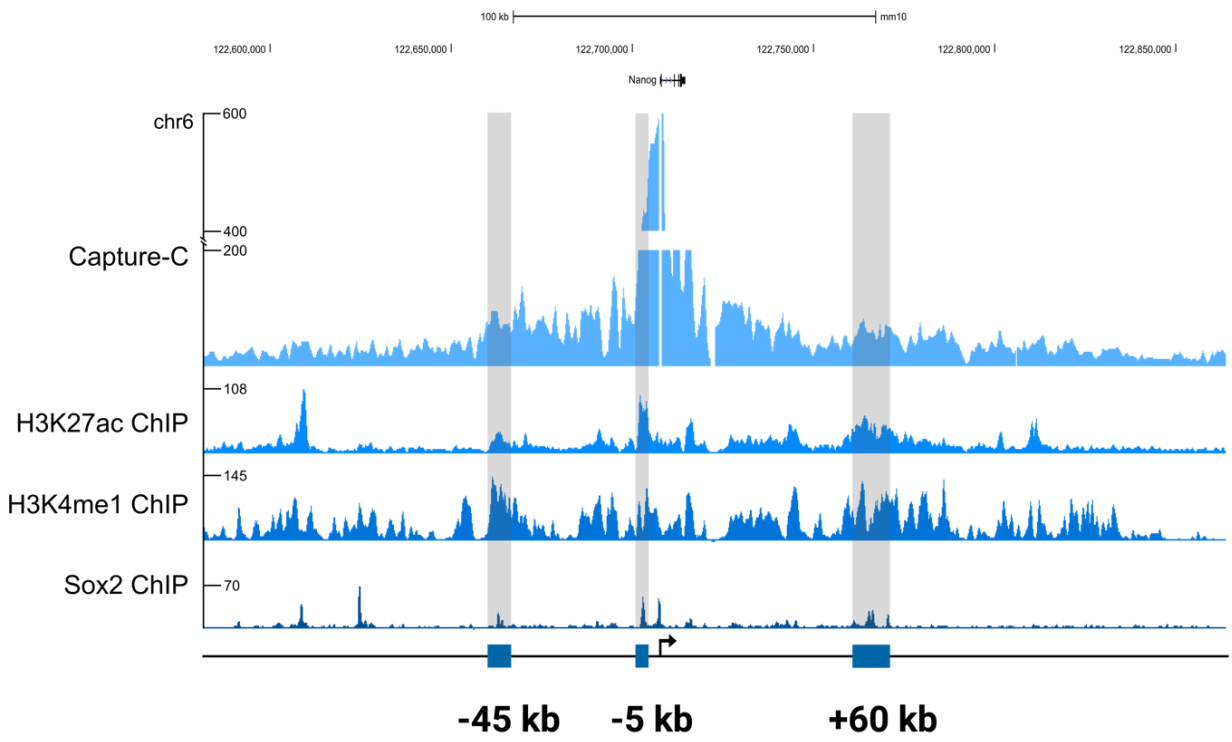

Supplementary Fig 11. The *Nanog* promoter interacts with three enhancer regions. Contact points between *Nanog* promoter and enhancer regions (significant interactions when score >= 5) using Capture-C analysis. The highlighted regions (grey) correspond to -45 kb, -5 kb and +60 kb *Nanog* enhancers.

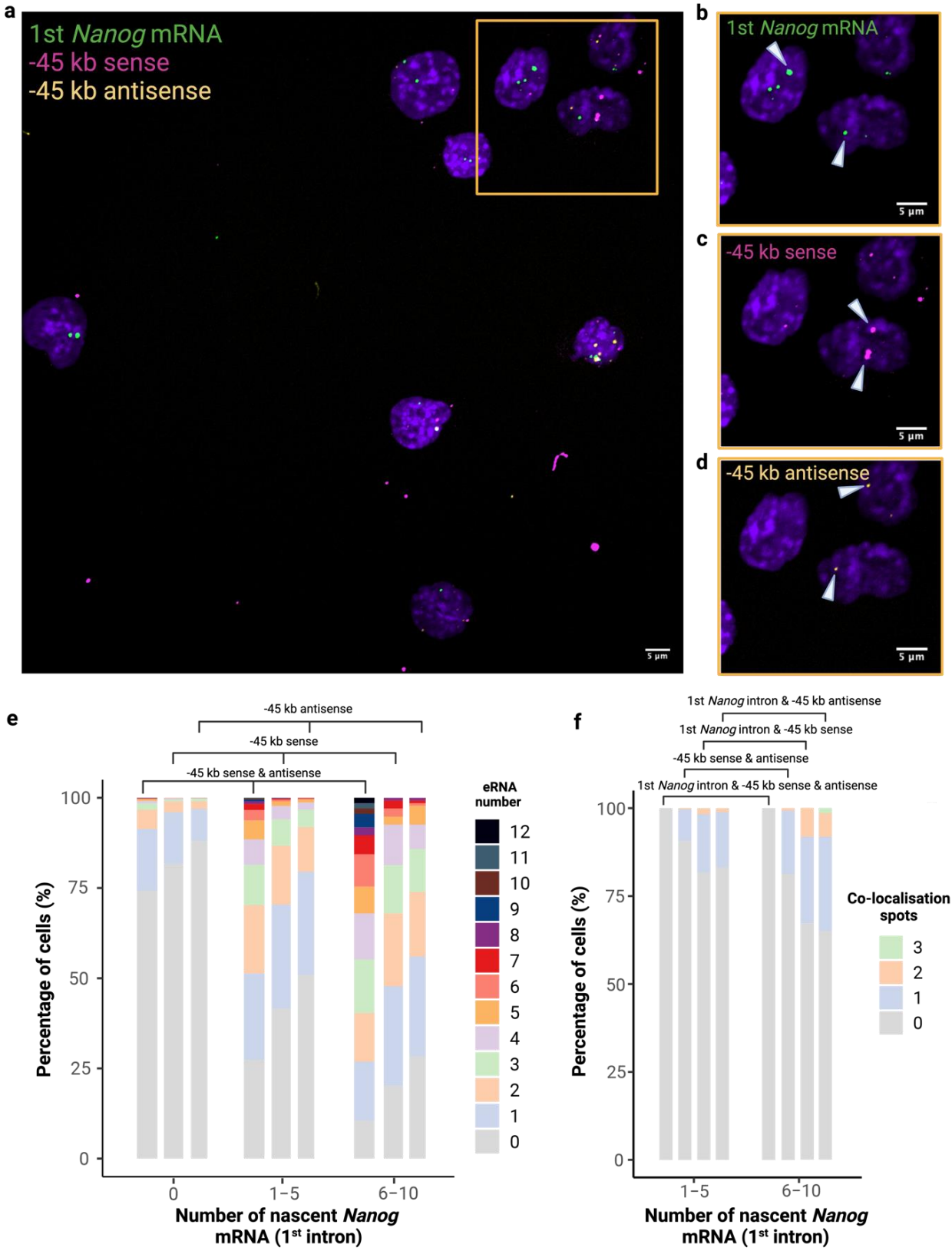

Supplementary Fig 12. Quantification of *Nanog* -45 kb eRNAs expression relative to *Nanog* mRNA first intron synthesis in mESCs population. (a) Microscope image showing the fluorescent signal of first intron *Nanog* mRNA (green), *Nanog* -45 kb sense (magenta) and antisense (yellow) eRNAs captured from mESCs. **(b-d)** Zoomed-in images (orange inset) showing individual fluorescent signal of first intron *Nanog* mRNA and eRNAs respectively. White arrowheads point to where eRNA spots were observed. **(e)** Quantitation of *Nanog* -45 kb sense and antisense eRNAs co-

expression with first intron *Nanog* mRNA shows a positive correlation between enhancer and gene body transcription. **(f)** Quantitation of *Nanog* -45 kb sense and antisense eRNAs co-localisation with first intron *Nanog* mRNA suggests that enhancers are lowly transcribed while *Nanog* mRNA is produced.

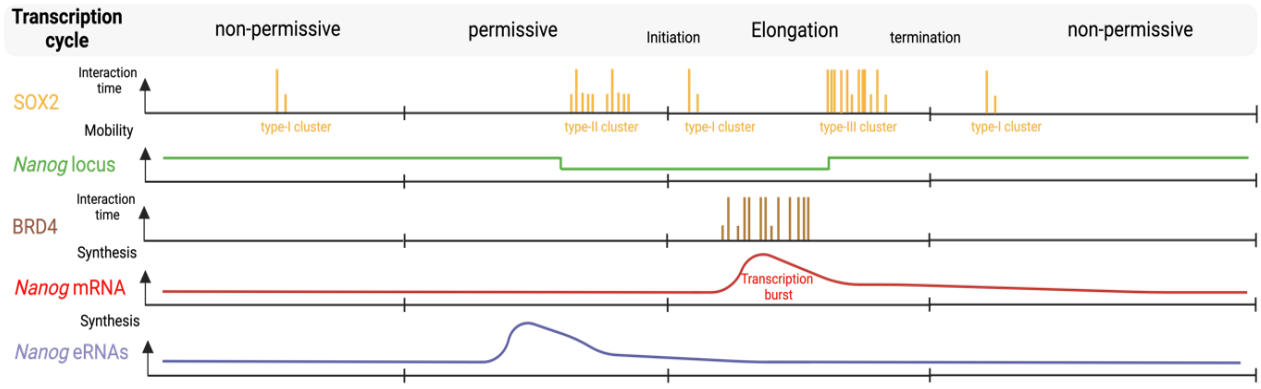

Supplementary Fig 13. Schematic representation of the regulatory factors' kinetics at the *Nanog* locus relative to its transcription cycle. The clustering activity (SOX2, orange and BRD4, brown), locus diffusion (green), mRNA synthesis (red) and *Nanog* eRNAs synthesis (purple). SOX2 type II burst events occur before the elongation step (locus with lower mobility when SOX2 bound), by contrast, type III burst events occur after the elongation step (locus with higher mobility when SOX2 bound).

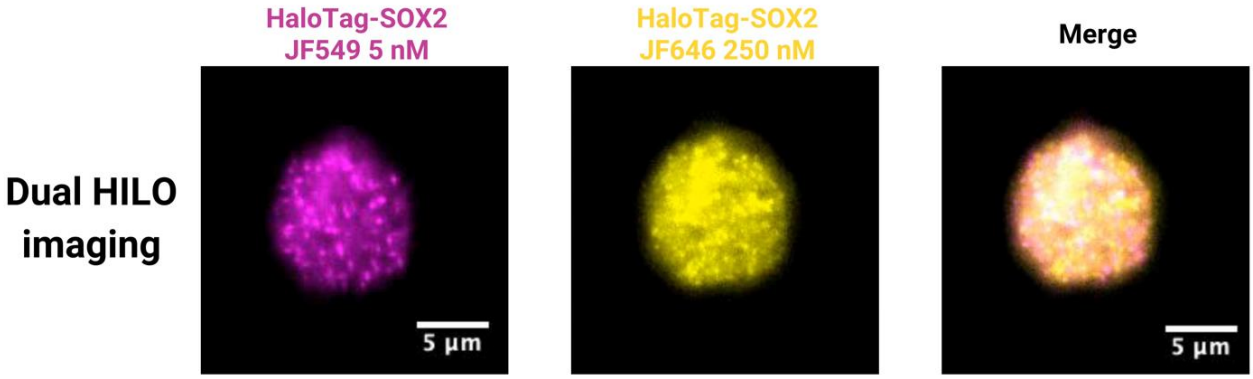

Supplementary Video 1. Simultaneous dual-channel imaging for SOX2 clustering events. Fluorescent signals from the sparse labelling HaloTag-SOX2 (magenta) and saturated labelling HaloTag-SOX2 (yellow). Merged video displaying the signal from both channels.

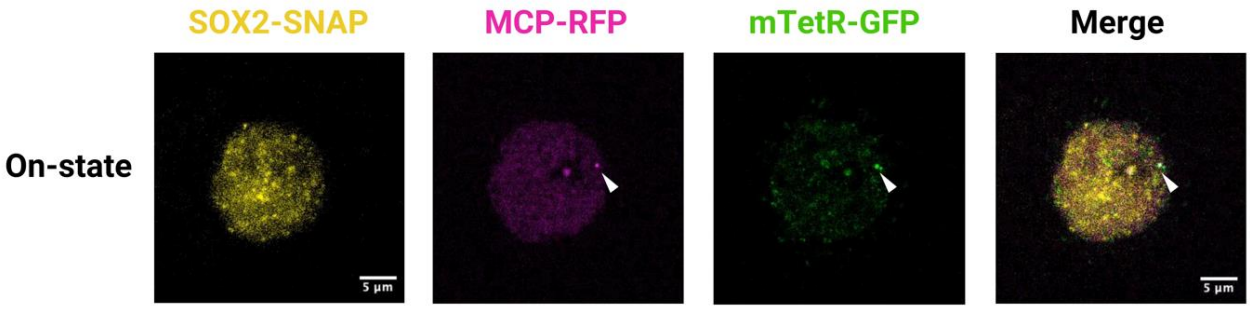

Supplementary Video 2. Multimodal live imaging of on-state cells using mode 1 image

acquisition method. Fluorescent signals from the *Nanog* locus (GFP, green), *Nanog* mRNA (RFP, magenta) and SOX2-SNAPtag SMT (yellow). Merged video displaying the signal from all channels with the spatial alignment. White arrowheads indicate locations where MCP-RFP and mTetR-GFP spots were observed simultaneously.

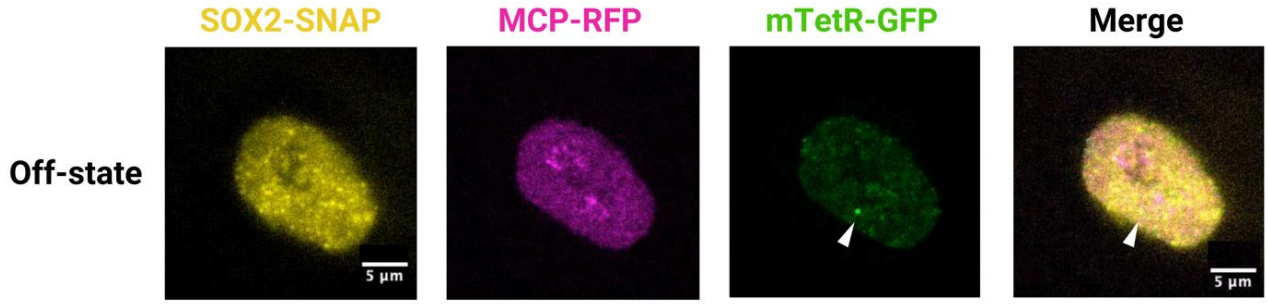

Supplementary Video 3. Multimodal live imaging of off-state cells (low SOX2 visiting frequency) using image acquisition mode 1. Fluorescent signals from the *Nanog* locus (GFP, green), *Nanog* mRNA (RFP, magenta) and SOX2-SNAP SMT (yellow). Merged video displaying the signal from all channels with the spatial alignment. White arrowheads point to the location where the mTetR-GFP spot was observed.

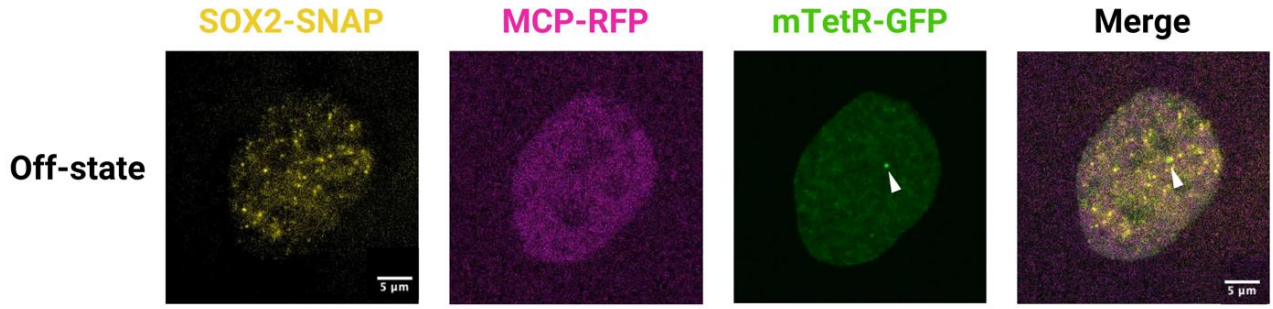

Supplementary Video 4. Multimodal live imaging of off-state cells (moderate SOX2 visiting frequency) using image acquisition mode 1. Fluorescent signals from the *Nanog* locus (GFP, green), *Nanog* mRNA (RFP, magenta) and SOX2-SNAP SMT (yellow). Merged video displaying the signal from all channels with the spatial alignment. White arrowheads point to the location where the mTetR-GFP spot was observed.

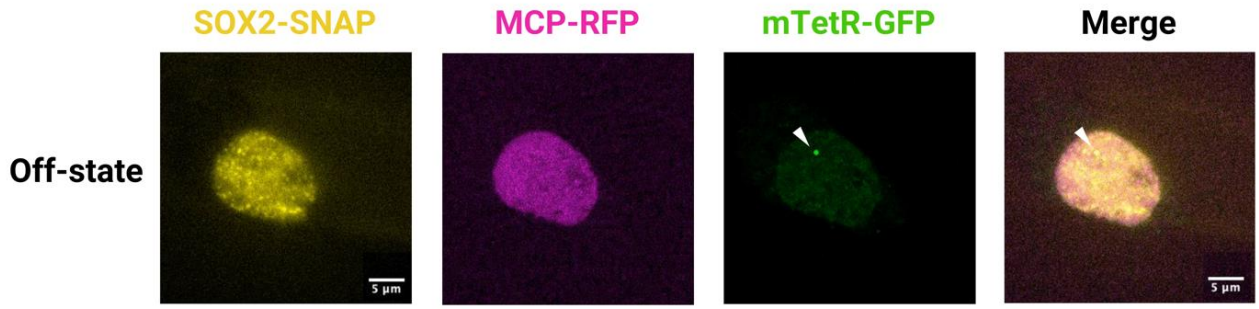

Supplementary Video 5. Multimodal live imaging of off-state cells (high SOX2 visiting frequency) using image acquisition mode 1. Fluorescent signals from the *Nanog* locus (GFP, green), *Nanog* mRNA (RFP, magenta) and SOX2-SNAPtag SMT (yellow). Merged video displaying

the signal from all channels with the spatial alignment. White arrowheads point to the location where the mTetR-GFP spot was observed.

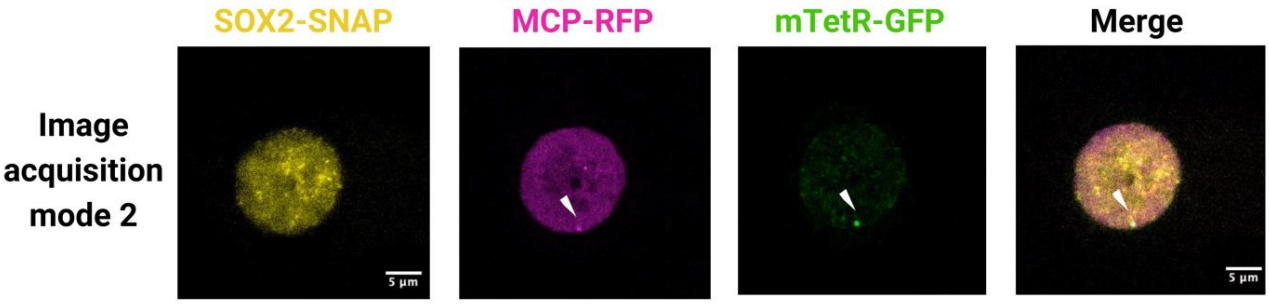

Supplementary Video 6. Multimodal live imaging of cells using mode 2 image acquisition method. This type of imaging acquisition contains both an on-state and an off-state. Fluorescent signals from the *Nanog* locus (GFP, green), *Nanog* mRNA (RFP, magenta) and SOX2-SNAPtag SMT (yellow). Merged video displaying the signal from all channels with the spatial alignment. White arrowheads indicate locations where MCP-RFP and mTetR-GFP spots were observed simultaneously.

Data and materials availability: All data are available in the main text or the supplementary materials and have been deposited to Datadryad for access to raw files.

Accession number and link: https://doi.org/10.5061/dryad.wpzgmsbw4